

FAA WJH Technical Center
00090611

THEORETICAL RELATIONSHIPS BETWEEN MODULI FOR SOIL LAYERS BENEATH CONCRETE PAVEMENTS

**John E. Crawford
Jerome S. Hopkins
James Smith**

**Civil Engineering Laboratory
Naval Construction Battalion Center
Port Hueneme, Calif. 93043**



**NAFEC
LIBRARY
MAY 13 '76**

May 1976

FINAL REPORT

Document is available to the public through the
National Technical Information Service,
Springfield, Virginia 22151

Prepared for

**U.S. DEPARTMENT OF TRANSPORTATION
FEDERAL AVIATION ADMINISTRATION
Systems Research & Development Service
Washington, D.C. 20590**

NOTICES

This document is disseminated under the sponsorship of the Department of Transportation in the interest of information exchange. The United States Government assumes no liability for its contents or use thereof.

The United States Government does not endorse products or manufacturers. Trade or manufacturers' names appear herein solely because they are considered essential to the object of this report.

1. Report No. FAA-RD-75-140		2. Government Accession No.		3. Recipient's Catalog No.	
4. Title and Subtitle Theoretical Relationships Between Moduli for Soil Layers Beneath Concrete Pavements				5. Report Date May 1976	
				6. Performing Organization Code	
7. Author(s) John E. Crawford, Jerome S. Hopkins, and James Smith				8. Performing Organization Report No.	
9. Performing Organization Name and Address Civil Engineering Laboratory Naval Construction Battalion Center Port Huene, California 93043				10. Work Unit No. (TRIS)	
				11. Contract or Grant No. DOT FA74WAI-487	
12. Sponsoring Agency Name and Address U.S. Department of Transportation Federal Aviation Administration Washington, D.C.				13. Type of Report and Period Covered Final report June 1974 -- March 1975	
				14. Sponsoring Agency Code ARD-430	
15. Supplementary Notes					
16. Abstract Several mathematical relationships are presented which relate the Westergaard method of analysis used for rigid pavements and the elastic layer method of analysis used for both rigid and flexible pavements. Twenty-three pavement sections were selected to illustrate the usage of these relationships. These sections represent the widest possible variation of rigid pavement types for which sufficient materials data was available. For the sections studied and within the context of linear analysis, these relationships demonstrate that the peak pavement stress can usually be computed by either method of analysis while the peak displacements are separated by a rather consistent seventy percent.					
17. Key Words Airport pavements Pavement design Pavement response Rigid pavements			18. Distribution Statement Document is available to the public through the National Technical Information Service Springfield, VA 22151		
19. Security Classif. (of this report) Unclassified		20. Security Classif. (of this page) Unclassified		21. No. of Pages 68	22. Price

METRIC CONVERSION FACTORS

Approximate Conversions to Metric Measures

Symbol	When You Know	Multiply by	To Find	Symbol
LENGTH				
in	inches	2.5	centimeters	cm
ft	feet	30	centimeters	cm
yd	yards	0.9	meters	m
mi	miles	1.6	kilometers	km
AREA				
in ²	square inches	6.5	square centimeters	cm ²
ft ²	square feet	0.09	square meters	m ²
yd ²	square yards	0.8	square meters	m ²
mi ²	square miles	2.6	square kilometers	km ²
	acres	0.4	hectares	ha
MASS (weight)				
oz	ounces	28	grams	g
lb	pounds	0.45	kilograms	kg
	short tons (2000 lb)	0.9	tonnes	t
VOLUME				
tsp	teaspoons	5	milliliters	ml
Tbsp	tablespoons	15	milliliters	ml
fl oz	fluid ounces	30	milliliters	ml
c	cups	0.24	liters	l
pt	pints	0.47	liters	l
qt	quarts	0.95	liters	l
gal	gallons	3.8	liters	l
ft ³	cubic feet	0.03	cubic meters	m ³
yd ³	cubic yards	0.76	cubic meters	m ³
TEMPERATURE (exact)				
°F	Fahrenheit temperature	5/9 after subtracting 32!	Celsius temperature	°C

* 1 in = 2.54 exactly. For other exact conversions, see Appendix 1 for tables. (See NBS Misc. Publ. 220, Units of Weights and Measures, Page 32, DE-33, Data 1.1, 1.2, 1.3, 1.4, 1.5, 1.6, 1.7, 1.8, 1.9, 2.0, 2.1, 2.2, 2.3, 2.4, 2.5, 2.6, 2.7, 2.8, 2.9, 3.0, 3.1, 3.2, 3.3, 3.4, 3.5, 3.6, 3.7, 3.8, 3.9, 4.0, 4.1, 4.2, 4.3, 4.4, 4.5, 4.6, 4.7, 4.8, 4.9, 5.0, 5.1, 5.2, 5.3, 5.4, 5.5, 5.6, 5.7, 5.8, 5.9, 6.0, 6.1, 6.2, 6.3, 6.4, 6.5, 6.6, 6.7, 6.8, 6.9, 7.0, 7.1, 7.2, 7.3, 7.4, 7.5, 7.6, 7.7, 7.8, 7.9, 8.0, 8.1, 8.2, 8.3, 8.4, 8.5, 8.6, 8.7, 8.8, 8.9, 9.0, 9.1, 9.2, 9.3, 9.4, 9.5, 9.6, 9.7, 9.8, 9.9, 10.0, 10.1, 10.2, 10.3, 10.4, 10.5, 10.6, 10.7, 10.8, 10.9, 11.0, 11.1, 11.2, 11.3, 11.4, 11.5, 11.6, 11.7, 11.8, 11.9, 12.0, 12.1, 12.2, 12.3, 12.4, 12.5, 12.6, 12.7, 12.8, 12.9, 13.0, 13.1, 13.2, 13.3, 13.4, 13.5, 13.6, 13.7, 13.8, 13.9, 14.0, 14.1, 14.2, 14.3, 14.4, 14.5, 14.6, 14.7, 14.8, 14.9, 15.0, 15.1, 15.2, 15.3, 15.4, 15.5, 15.6, 15.7, 15.8, 15.9, 16.0, 16.1, 16.2, 16.3, 16.4, 16.5, 16.6, 16.7, 16.8, 16.9, 17.0, 17.1, 17.2, 17.3, 17.4, 17.5, 17.6, 17.7, 17.8, 17.9, 18.0, 18.1, 18.2, 18.3, 18.4, 18.5, 18.6, 18.7, 18.8, 18.9, 19.0, 19.1, 19.2, 19.3, 19.4, 19.5, 19.6, 19.7, 19.8, 19.9, 20.0, 20.1, 20.2, 20.3, 20.4, 20.5, 20.6, 20.7, 20.8, 20.9, 21.0, 21.1, 21.2, 21.3, 21.4, 21.5, 21.6, 21.7, 21.8, 21.9, 22.0, 22.1, 22.2, 22.3, 22.4, 22.5, 22.6, 22.7, 22.8, 22.9, 23.0, 23.1, 23.2, 23.3, 23.4, 23.5, 23.6, 23.7, 23.8, 23.9, 24.0, 24.1, 24.2, 24.3, 24.4, 24.5, 24.6, 24.7, 24.8, 24.9, 25.0, 25.1, 25.2, 25.3, 25.4, 25.5, 25.6, 25.7, 25.8, 25.9, 26.0, 26.1, 26.2, 26.3, 26.4, 26.5, 26.6, 26.7, 26.8, 26.9, 27.0, 27.1, 27.2, 27.3, 27.4, 27.5, 27.6, 27.7, 27.8, 27.9, 28.0, 28.1, 28.2, 28.3, 28.4, 28.5, 28.6, 28.7, 28.8, 28.9, 29.0, 29.1, 29.2, 29.3, 29.4, 29.5, 29.6, 29.7, 29.8, 29.9, 30.0, 30.1, 30.2, 30.3, 30.4, 30.5, 30.6, 30.7, 30.8, 30.9, 31.0, 31.1, 31.2, 31.3, 31.4, 31.5, 31.6, 31.7, 31.8, 31.9, 32.0, 32.1, 32.2, 32.3, 32.4, 32.5, 32.6, 32.7, 32.8, 32.9, 33.0, 33.1, 33.2, 33.3, 33.4, 33.5, 33.6, 33.7, 33.8, 33.9, 34.0, 34.1, 34.2, 34.3, 34.4, 34.5, 34.6, 34.7, 34.8, 34.9, 35.0, 35.1, 35.2, 35.3, 35.4, 35.5, 35.6, 35.7, 35.8, 35.9, 36.0, 36.1, 36.2, 36.3, 36.4, 36.5, 36.6, 36.7, 36.8, 36.9, 37.0, 37.1, 37.2, 37.3, 37.4, 37.5, 37.6, 37.7, 37.8, 37.9, 38.0, 38.1, 38.2, 38.3, 38.4, 38.5, 38.6, 38.7, 38.8, 38.9, 39.0, 39.1, 39.2, 39.3, 39.4, 39.5, 39.6, 39.7, 39.8, 39.9, 40.0, 40.1, 40.2, 40.3, 40.4, 40.5, 40.6, 40.7, 40.8, 40.9, 41.0, 41.1, 41.2, 41.3, 41.4, 41.5, 41.6, 41.7, 41.8, 41.9, 42.0, 42.1, 42.2, 42.3, 42.4, 42.5, 42.6, 42.7, 42.8, 42.9, 43.0, 43.1, 43.2, 43.3, 43.4, 43.5, 43.6, 43.7, 43.8, 43.9, 44.0, 44.1, 44.2, 44.3, 44.4, 44.5, 44.6, 44.7, 44.8, 44.9, 45.0, 45.1, 45.2, 45.3, 45.4, 45.5, 45.6, 45.7, 45.8, 45.9, 46.0, 46.1, 46.2, 46.3, 46.4, 46.5, 46.6, 46.7, 46.8, 46.9, 47.0, 47.1, 47.2, 47.3, 47.4, 47.5, 47.6, 47.7, 47.8, 47.9, 48.0, 48.1, 48.2, 48.3, 48.4, 48.5, 48.6, 48.7, 48.8, 48.9, 49.0, 49.1, 49.2, 49.3, 49.4, 49.5, 49.6, 49.7, 49.8, 49.9, 50.0, 50.1, 50.2, 50.3, 50.4, 50.5, 50.6, 50.7, 50.8, 50.9, 51.0, 51.1, 51.2, 51.3, 51.4, 51.5, 51.6, 51.7, 51.8, 51.9, 52.0, 52.1, 52.2, 52.3, 52.4, 52.5, 52.6, 52.7, 52.8, 52.9, 53.0, 53.1, 53.2, 53.3, 53.4, 53.5, 53.6, 53.7, 53.8, 53.9, 54.0, 54.1, 54.2, 54.3, 54.4, 54.5, 54.6, 54.7, 54.8, 54.9, 55.0, 55.1, 55.2, 55.3, 55.4, 55.5, 55.6, 55.7, 55.8, 55.9, 56.0, 56.1, 56.2, 56.3, 56.4, 56.5, 56.6, 56.7, 56.8, 56.9, 57.0, 57.1, 57.2, 57.3, 57.4, 57.5, 57.6, 57.7, 57.8, 57.9, 58.0, 58.1, 58.2, 58.3, 58.4, 58.5, 58.6, 58.7, 58.8, 58.9, 59.0, 59.1, 59.2, 59.3, 59.4, 59.5, 59.6, 59.7, 59.8, 59.9, 60.0, 60.1, 60.2, 60.3, 60.4, 60.5, 60.6, 60.7, 60.8, 60.9, 61.0, 61.1, 61.2, 61.3, 61.4, 61.5, 61.6, 61.7, 61.8, 61.9, 62.0, 62.1, 62.2, 62.3, 62.4, 62.5, 62.6, 62.7, 62.8, 62.9, 63.0, 63.1, 63.2, 63.3, 63.4, 63.5, 63.6, 63.7, 63.8, 63.9, 64.0, 64.1, 64.2, 64.3, 64.4, 64.5, 64.6, 64.7, 64.8, 64.9, 65.0, 65.1, 65.2, 65.3, 65.4, 65.5, 65.6, 65.7, 65.8, 65.9, 66.0, 66.1, 66.2, 66.3, 66.4, 66.5, 66.6, 66.7, 66.8, 66.9, 67.0, 67.1, 67.2, 67.3, 67.4, 67.5, 67.6, 67.7, 67.8, 67.9, 68.0, 68.1, 68.2, 68.3, 68.4, 68.5, 68.6, 68.7, 68.8, 68.9, 69.0, 69.1, 69.2, 69.3, 69.4, 69.5, 69.6, 69.7, 69.8, 69.9, 70.0, 70.1, 70.2, 70.3, 70.4, 70.5, 70.6, 70.7, 70.8, 70.9, 71.0, 71.1, 71.2, 71.3, 71.4, 71.5, 71.6, 71.7, 71.8, 71.9, 72.0, 72.1, 72.2, 72.3, 72.4, 72.5, 72.6, 72.7, 72.8, 72.9, 73.0, 73.1, 73.2, 73.3, 73.4, 73.5, 73.6, 73.7, 73.8, 73.9, 74.0, 74.1, 74.2, 74.3, 74.4, 74.5, 74.6, 74.7, 74.8, 74.9, 75.0, 75.1, 75.2, 75.3, 75.4, 75.5, 75.6, 75.7, 75.8, 75.9, 76.0, 76.1, 76.2, 76.3, 76.4, 76.5, 76.6, 76.7, 76.8, 76.9, 77.0, 77.1, 77.2, 77.3, 77.4, 77.5, 77.6, 77.7, 77.8, 77.9, 78.0, 78.1, 78.2, 78.3, 78.4, 78.5, 78.6, 78.7, 78.8, 78.9, 79.0, 79.1, 79.2, 79.3, 79.4, 79.5, 79.6, 79.7, 79.8, 79.9, 80.0, 80.1, 80.2, 80.3, 80.4, 80.5, 80.6, 80.7, 80.8, 80.9, 81.0, 81.1, 81.2, 81.3, 81.4, 81.5, 81.6, 81.7, 81.8, 81.9, 82.0, 82.1, 82.2, 82.3, 82.4, 82.5, 82.6, 82.7, 82.8, 82.9, 83.0, 83.1, 83.2, 83.3, 83.4, 83.5, 83.6, 83.7, 83.8, 83.9, 84.0, 84.1, 84.2, 84.3, 84.4, 84.5, 84.6, 84.7, 84.8, 84.9, 85.0, 85.1, 85.2, 85.3, 85.4, 85.5, 85.6, 85.7, 85.8, 85.9, 86.0, 86.1, 86.2, 86.3, 86.4, 86.5, 86.6, 86.7, 86.8, 86.9, 87.0, 87.1, 87.2, 87.3, 87.4, 87.5, 87.6, 87.7, 87.8, 87.9, 88.0, 88.1, 88.2, 88.3, 88.4, 88.5, 88.6, 88.7, 88.8, 88.9, 89.0, 89.1, 89.2, 89.3, 89.4, 89.5, 89.6, 89.7, 89.8, 89.9, 90.0, 90.1, 90.2, 90.3, 90.4, 90.5, 90.6, 90.7, 90.8, 90.9, 91.0, 91.1, 91.2, 91.3, 91.4, 91.5, 91.6, 91.7, 91.8, 91.9, 92.0, 92.1, 92.2, 92.3, 92.4, 92.5, 92.6, 92.7, 92.8, 92.9, 93.0, 93.1, 93.2, 93.3, 93.4, 93.5, 93.6, 93.7, 93.8, 93.9, 94.0, 94.1, 94.2, 94.3, 94.4, 94.5, 94.6, 94.7, 94.8, 94.9, 95.0, 95.1, 95.2, 95.3, 95.4, 95.5, 95.6, 95.7, 95.8, 95.9, 96.0, 96.1, 96.2, 96.3, 96.4, 96.5, 96.6, 96.7, 96.8, 96.9, 97.0, 97.1, 97.2, 97.3, 97.4, 97.5, 97.6, 97.7, 97.8, 97.9, 98.0, 98.1, 98.2, 98.3, 98.4, 98.5, 98.6, 98.7, 98.8, 98.9, 99.0, 99.1, 99.2, 99.3, 99.4, 99.5, 99.6, 99.7, 99.8, 99.9, 100.0, 100.1, 100.2, 100.3, 100.4, 100.5, 100.6, 100.7, 100.8, 100.9, 101.0, 101.1, 101.2, 101.3, 101.4, 101.5, 101.6, 101.7, 101.8, 101.9, 102.0, 102.1, 102.2, 102.3, 102.4, 102.5, 102.6, 102.7, 102.8, 102.9, 103.0, 103.1, 103.2, 103.3, 103.4, 103.5, 103.6, 103.7, 103.8, 103.9, 104.0, 104.1, 104.2, 104.3, 104.4, 104.5, 104.6, 104.7, 104.8, 104.9, 105.0, 105.1, 105.2, 105.3, 105.4, 105.5, 105.6, 105.7, 105.8, 105.9, 106.0, 106.1, 106.2, 106.3, 106.4, 106.5, 106.6, 106.7, 106.8, 106.9, 107.0, 107.1, 107.2, 107.3, 107.4, 107.5, 107.6, 107.7, 107.8, 107.9, 108.0, 108.1, 108.2, 108.3, 108.4, 108.5, 108.6, 108.7, 108.8, 108.9, 109.0, 109.1, 109.2, 109.3, 109.4, 109.5, 109.6, 109.7, 109.8, 109.9, 110.0, 110.1, 110.2, 110.3, 110.4, 110.5, 110.6, 110.7, 110.8, 110.9, 111.0, 111.1, 111.2, 111.3, 111.4, 111.5, 111.6, 111.7, 111.8, 111.9, 112.0, 112.1, 112.2, 112.3, 112.4, 112.5, 112.6, 112.7, 112.8, 112.9, 113.0, 113.1, 113.2, 113.3, 113.4, 113.5, 113.6, 113.7, 113.8, 113.9, 114.0, 114.1, 114.2, 114.3, 114.4, 114.5, 114.6, 114.7, 114.8, 114.9, 115.0, 115.1, 115.2, 115.3, 115.4, 115.5, 115.6, 115.7, 115.8, 115.9, 116.0, 116.1, 116.2, 116.3, 116.4, 116.5, 116.6, 116.7, 116.8, 116.9, 117.0, 117.1, 117.2, 117.3, 117.4, 117.5, 117.6, 117.7, 117.8, 117.9, 118.0, 118.1, 118.2, 118.3, 118.4, 118.5, 118.6, 118.7, 118.8, 118.9, 119.0, 119.1, 119.2, 119.3, 119.4, 119.5, 119.6, 119.7, 119.8, 119.9, 120.0, 120.1, 120.2, 120.3, 120.4, 120.5, 120.6, 120.7, 120.8, 120.9, 121.0, 121.1, 121.2, 121.3, 121.4, 121.5, 121.6, 121.7, 121.8, 121.9, 122.0, 122.1, 122.2, 122.3, 122.4, 122.5, 122.6, 122.7, 122.8, 122.9, 123.0, 123.1, 123.2, 123.3, 123.4, 123.5, 123.6, 123.7, 123.8, 123.9, 124.0, 124.1, 124.2, 124.3, 124.4, 124.5, 124.6, 124.7, 124.8, 124.9, 125.0, 125.1, 125.2, 125.3, 125.4, 125.5, 125.6, 125.7, 125.8, 125.9, 126.0, 126.1, 126.2, 126.3, 126.4, 126.5, 126.6, 126.7, 126.8, 126.9, 127.0, 127.1, 127.2, 127.3, 127.4, 127.5, 127.6, 127.7, 127.8, 127.9, 128.0, 128.1, 128.2, 128.3, 128.4, 128.5, 128.6, 128.7, 128.8, 128.9, 129.0, 129.1, 129.2, 129.3, 129.4, 129.5, 129.6, 129.7, 129.8, 129.9, 130.0, 130.1, 130.2, 130.3, 130.4, 130.5, 130.6, 130.7, 130.8, 130.9, 131.0, 131.1, 131.2, 131.3, 131.4, 131.5, 131.6, 131.7, 131.8, 131.9, 132.0, 132.1, 132.2, 132.3, 132.4, 132.5, 132.6, 132.7, 132.8, 132.9, 133.0, 133.1, 133.2, 133.3, 133.4, 133.5, 133.6, 133.7, 133.8, 133.9, 134.0, 134.1, 134.2, 134.3, 134.4, 134.5, 134.6, 134.7, 134.8, 134.9, 135.0, 135.1, 135.2, 135.3, 135.4, 135.5, 135.6, 135.7, 135.8, 135.9, 136.0, 136.1, 136.2, 136.3, 136.4, 136.5, 136.6, 136.7, 136.8, 136.9, 137.0, 137.1, 137.2, 137.3, 137.4, 137.5, 137.6, 137.7, 137.8, 137.9, 138.0, 138.1, 138.2, 138.3, 138.4, 138.5, 138.6, 138.7, 138.8, 138.9, 139.0, 139.1, 139.2, 139.3, 139.4, 139.5, 139.6, 139.7, 139.8, 139.9, 140.0, 140.1, 140.2, 140.3, 140.4, 140.5, 140.6, 140.7, 140.8, 140.9, 141.0, 141.1, 141.2, 141.3, 141.4, 141.5, 141.6, 141.7, 141.8, 141.9, 142.0, 142.1, 142.2, 142.3, 142.4, 142.5, 142.6, 142.7, 142.8, 142.9, 143.0, 143.1, 143.2, 143.3, 143.4, 143.5, 143.6, 143.7, 143.8, 143.9, 144.0, 144.1, 144.2, 144.3, 144.4, 144.5, 144.6, 144.7, 144.8, 144.9, 145.0, 145.1, 145.2, 145.3, 145.4, 145.5, 145.6, 145.7, 145.8, 145.9, 146.0, 146.1, 146.2, 146.3, 146.4, 146.5, 146.6, 146.7, 146.8, 146.9, 147.0, 147.1, 147.2, 147.3, 147.4, 147.5, 147.6, 147.7, 147.8, 147.9, 148.0, 148.1, 148.2, 148.3, 148.4, 148.5, 148.6, 148.7, 148.8, 148.9, 149.0, 149.1, 149.2, 149.3, 149.4, 149.5, 149.6, 149.7, 149.8, 149.9, 150.0, 150.1, 150.2, 150.3, 150.4, 150.5, 150.6, 150.7, 150.8, 150.9, 151.0, 151.1, 151.2, 151.3, 151.4, 151.5, 151.6, 151.7, 151.8, 151.9, 152.0, 152.1, 152.2, 152.3, 152.4, 152.5, 152.6, 152.7, 152.8, 152.9, 153.0, 153.1, 153.2, 153.3, 153.4, 153.5, 153.6, 153.7, 153.8, 153.9, 154.0, 154.1, 154.2, 154.3, 154.4, 154.5, 154.6, 154.7, 154.8, 154.9, 155.0, 155.1, 155.2, 155.3, 155.4, 155.5, 155.6, 155.7, 155.8, 155.9, 156.0, 156.1, 156.2, 156.3, 156.4, 156.5, 156.6, 156.7, 156.8, 156.9, 157.0, 157.1, 157.2, 157.3, 157.4, 157.5, 157.6, 157.7, 157.8, 157.9, 158.0, 158.1, 158.2, 158.3, 158.4, 158.5, 158.6, 158.7, 158.8, 158.9, 159.0, 159.1, 159.2, 159.3, 159.4, 159.5, 159.6, 159.7, 159.8, 159.9, 160.0, 160.1, 160.2, 160.3, 160.4, 160.5, 160.6, 160.7, 160.8, 160.9, 161.0, 161.1, 161.2, 161.3, 161.4, 161.5, 161.6, 161.7, 161.8, 161.9, 162.0, 162.1, 162.2, 162.3, 162.4, 162.5, 162.6, 162.7, 162.8, 162.9, 163.0, 163.1, 163.2, 163.3, 163.4, 163.5, 163.6, 163.7, 163.8, 163.9, 164.0, 164.1, 164.2, 164.3, 164.4, 164.5, 164.6, 164.7, 164.8, 164.9, 165.0, 165.1, 165.2, 165.3, 165.4, 165.5, 165.6, 165.7, 165.8, 165.9, 166.0, 166.1, 166.2, 166.3, 166.4, 166.5, 166.6, 166.7, 166.8, 166.9, 167.0, 167.1, 167.2, 167.3, 167.4, 167.5, 167.6, 167.7, 167.8, 167.9, 168.0, 168.1, 168.2, 168.3, 168.4, 168.5, 168.6, 168.7, 168.8, 168.9, 169.0, 169.1, 169.2, 169.3, 169.4, 169.5, 169.6, 169.7, 169.8, 169.9, 170.0, 170.1, 170.2, 170.3, 170.4, 170.5, 170.6, 170.7, 170.8, 170.9, 171.0, 171.1, 171.2, 171.3, 171.4, 1

PREFACE

The study described in this report was sponsored by the Federal Aviation Administration under Inter-Agency Agreement No. DOT-FA74WAI-487. "Theoretical Relationship Between Moduli for Soil Layers Beneath Concrete Pavements." This report is the first of two reports to be completed under this agreement and covers the work accomplished between June 1974 and March 1975.

The kind assistance of the U. S. Army Engineer Waterways Experiment Station, especially Dr. Walter R. Barker and Dr. Frazier Parker, in gathering the data for Figure 5 of this report is appreciated. Also appreciated was the excellent guidance provided by Mr. H. Tomita of the Airport Pavement Branch of the Federal Aviation Administration.

LIST OF TABLES

	Page
Table 1. Results of Usage of Westergaard Functionals	16
Table 2. Results of Usage of Westergaard Functionals for F4 Load	17
Table 3. Accuracy Measures Associated With k_w^1	18
Table B-1. Mathematically Selected Pavement Sections	58
Table B-2. Comparison of Stress Functionals.	59

I. INTRODUCTION

The purpose of this report is to present a mathematically consistent relationship between the Westergaard method of analysis used for rigid pavements and the elastic layer method of analysis used for both rigid and flexible pavements. It is intended that this relationship provide an explanation for the different results which sometimes occur from application of these two methods to the same pavement. The relationship also demonstrates that the problem of correlating the two methods can usually be related to inconsistencies in material input, to one or both methods; and to a considerably lesser extent, to the disparities in the mathematical idealizations.

The means used to relate the elastic layer parameters to those of Westergaard rely on the fundamental laws of mechanics, on which both methods are based. To insure a common starting point, a brief description of the equations which are associated with Westergaard and elastic layer^a analyses, is presented. These analyses are based on two different linear idealizations of a pavement system.

The Westergaard idealization considers a plate of infinite extent supported by a fluid with a modulus of subgrade reaction k (Figure 1). A uniform pressure P is applied over a circular^b area of radius "a" to the top surface of the plate. The responses used by most engineers are the maximum deflection, which occurs under the center of the load, and the maximum horizontal tensile stress, which occurs under the center of the load at the bottom edge of the plate. The expressions for these responses obtained from Reference 1 are:

^a Sometimes referred to as Burmister type analyses, or, for a single layer, as Boussinesq analyses.
^b An elliptical formulation is also used, but is not considered in this report. Formulations are also available for edge and joint loadings, see Reference 1.

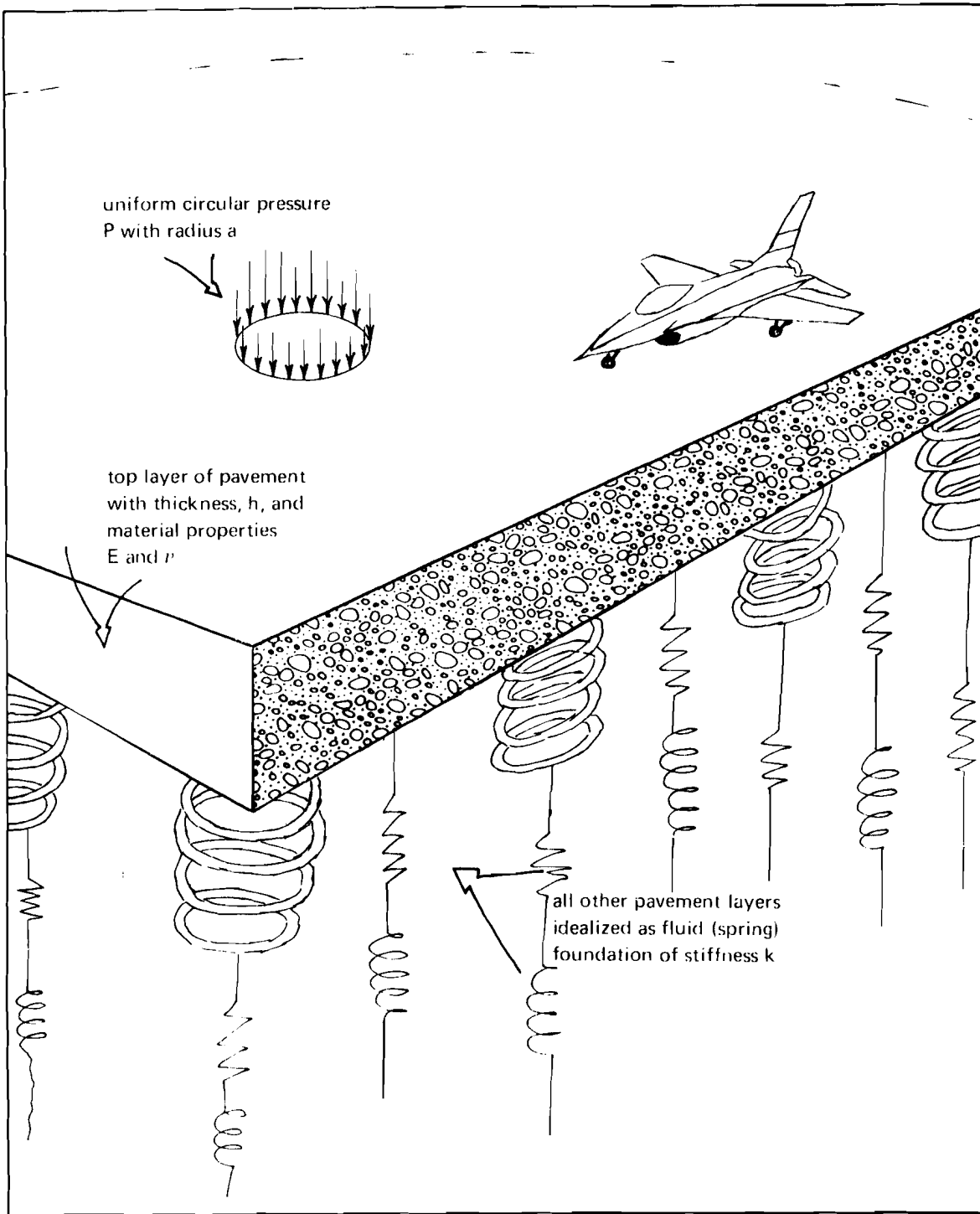


Figure 1. Westergaard pavement idealization.

$$\delta = \frac{P\pi a^2}{8kL^2} \left[1 - \frac{a^2}{8\pi L^2} \left(\ln \frac{Eh^3}{ka^4} \right) - \frac{3a^2}{8\pi L^2} \right] \quad (1)$$

$$\text{where } L^4 = \frac{Eh^3}{12(1 - \nu^2)k}$$

$$\sigma = \frac{3Pa^2}{8h^2} (1 + \nu) \left(\ln \frac{Eh^3}{ka^4} \right) \quad (2)$$

Traditionally, this idealization has been used to design rigid pavements.

The elastic layer idealization considers a semi-infinite body composed of N horizontal layers of homogeneous material (Figure 2). A uniform pressure P is applied over a circular area of radius "a" to the top surface of the top layer. Each layer is defined using Young's modulus E_n , Poisson's ratio ν_n , and layer thickness h_n^c . For the purposes of this report, only the responses similar to those of Westergaard are discussed, i.e., maximum deflection and tensile stress in the top layer. The expressions for these responses are:^d

$$\delta = \frac{Pa(1 + \nu_1)}{E_1} \int_0^\infty \left[A_1^1 + A_2^1(4\nu_1 - 2)(A_3^1 - A_4^1) \right] \frac{J_1(x)}{x} dx \quad (3)$$

^c All layers (i.e., $n = 1, 2, 3 \dots N$) extend laterally to infinity while the bottom layer extends vertically to infinity (i.e., $h_N = \infty$).

^d For a single layer system, consideration of which is deemed irrelevant to the current discussion, $\delta = Pa/E(1 - \nu^2)$ and $\sigma = 0$. Appendix A [i.e., equations (A-51 and A-50)] $w(0,0)$ and $\sigma_{rr}(0, h_1)$ are used.

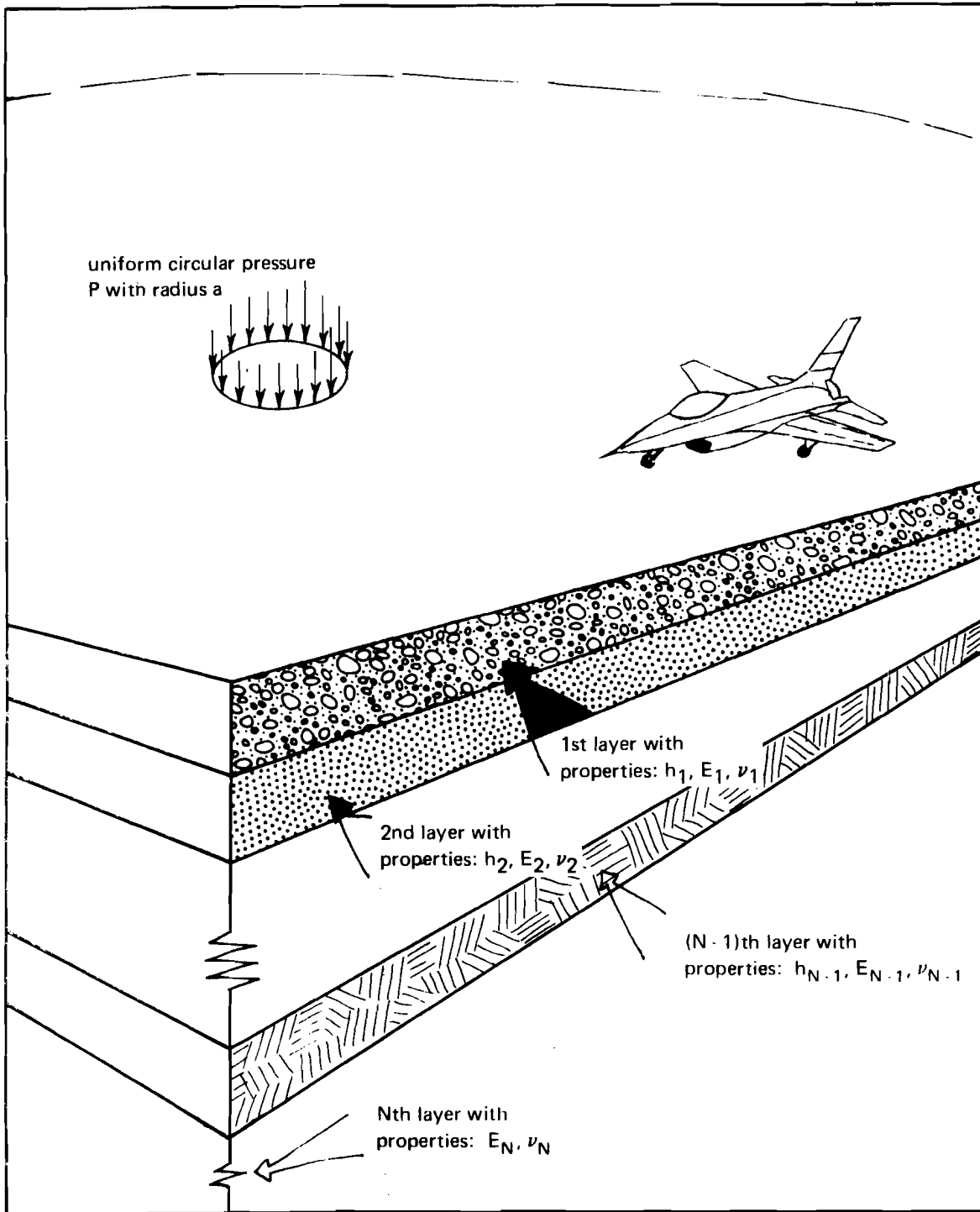


Figure 2. Elastic layer idealization.

$$\sigma = -\frac{p}{2} \int_0^{\infty} \left[A_5^1 - A_2^1 + (A_6^1 + A_4^1)(4\nu_1 + 1) + ph_1(A_6^1 - A_4^1) \right] e^{-ph_1} J_1(x) dx \quad (4)$$

where J_1 is a Bessel function

The derivation for these expressions, and the definitions of the constants $[A_1^1 \dots A_6^1]$ and transform parameter $[p]$ are presented in Appendix A^e. Computers and numerical procedures must be used to solve these complicated expressions. The ELAST computer program, which solves these two expressions, is described in Appendix C. Programs which solve for the general response of elastic layer systems are also available, but are more complicated and cost more to run^f [References 2, 3, and 4].

II. DEVELOPMENT OF RELATIONSHIP BETWEEN WESTERGAARD AND ELASTIC LAYER ANALYSES

Three different methods for computing "k" from an elastic layer system are described.

Method 1. Computation of k based on the simulation of a plate bearing test using an elastic layer idealization.

^e To be notationally consistent with equations (1 and 2), δ and σ are used here, while for the analogous equations in Appendix A [i.e., equations (A-51 and A-50)] $w(0,0)$ and $\sigma_{rr}(0,h_1)$ are used.

^f For example, ELAST runs on an average twenty five times faster than an equivalent run of the program BISTRO described in Reference 2.

Method 2. Computation of k based on the requirement that equations (1 and 3) produce the same values of displacement.

Method 3. Computation of k based on the requirement that equations (2 and 4) produce the same values of stress.

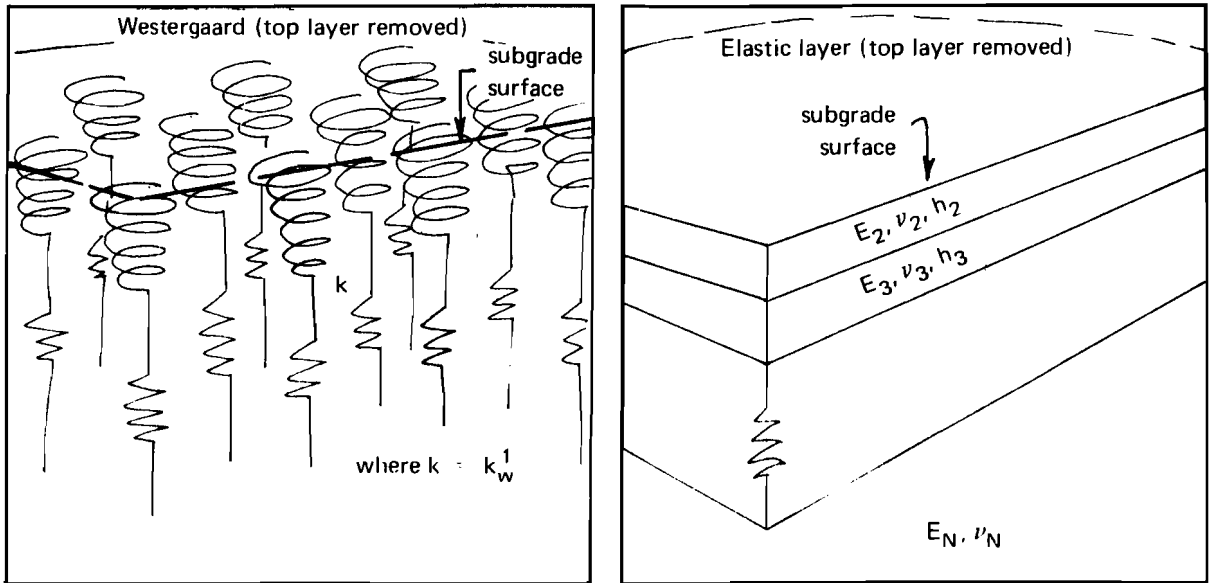
It is felt that these three methods comprise the significant ways to relate the Westergaard and elastic layer idealizations.

Ideally, for a specific pavement, the values of k produced by methods 1, 2, and 3, as well as that measured in the field, would be equal. However, due to the "vagaries" of nature, this is not to be. Discussion concerning the implication of these differences is given in this and the next section.

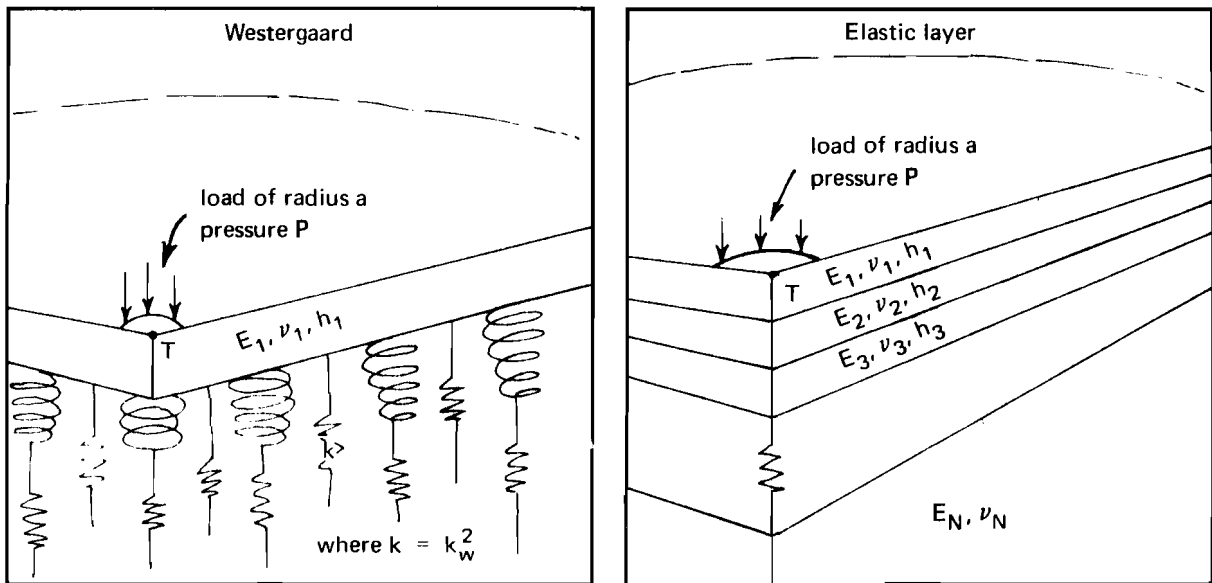
1. Westergaard Functionals

For conciseness, the mathematical implementations of methods 1, 2, and 3 are denoted as Westergaard functionals. From these functionals various values, mathematically equivalent to "k", are computed. These values provide quantitative measurements of the relationship between the two idealizations.

The Westergaard displacement functional implements Methods 1 and 2: denoted k_w^1 and k_w^2 . Figure 3a illustrates the application of k_w^1 . It shows two equivalent idealizations, where the Westergaard parameter is computed so that both subgrades have the same stiffness (i.e., $k = k_w^1$, where k_w^1 is a function of $E_2, \nu_2, h_2, E_3, \nu_3, h_3 \dots E_N, \nu_N$). Figure 3b shows two equivalent idealizations where the Westergaard parameter is computed so that both top layers have the same peak deflection (i.e., $k = k_w^2$, where k_w^2 is a function of $E_1, \nu_1, h_1, E_2, \nu_2, h_2 \dots E_N, \nu_N$).



(a) Idealizations for k_w^1 equivalency where the deflection at the subgrade surface caused by a load (which is uniformly distributed over a circle 30 inches in diameter) applied to the surface is the same for both idealizations.



(b) Idealizations for k_w^2 equivalency where the deflection at T for both idealizations is equal.

Figure 3. Usage of Westergaard displacement functionals.

Finally, to create an equivalency for maximum tensile stress in the top layer (Method 3), the Westergaard stress functional k_s^1 is provided (Figure 4).

k_w^1 functional. The k_w^1 functional is derived from an elastic layer idealization where the first layer is removed, and the surface of the second layer is loaded with pressure P of radius "a" as shown in Figure 3a. Equation (5) defines the peak deflection for this situation, and is taken from Equation (A-51) of Appendix A.

$$\delta_2 = \frac{Pa(1 + \nu_2)}{E_2} \int_0^{\infty} \left[A_1^2 + A_2^2(4\nu_2 - 2)(A_3^2 - A_4^2) \right] \frac{J_1(x)}{x} dx \quad (5)$$

where $[A_1^2, A_2^2, A_3^2, \text{ and } A_4^2]$ are functions of $[E_3, \nu_3, h_3, E_4, \nu_4, h_4, \dots, \nu_N]$

The definition of k is employed to obtain k_w^1 from equation (5), that is, the reciprocal of the deflection caused by a unit pressure applied over a 15-inch radius circle.

$$k_w^1 = \frac{1}{\delta_2} \quad (6)$$

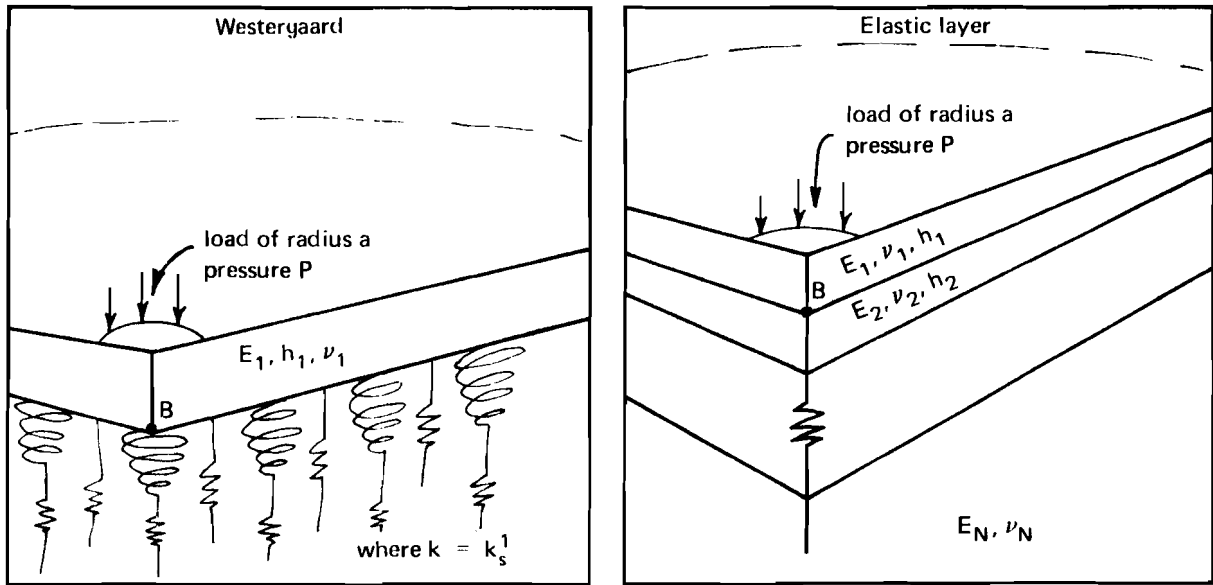
where δ_2 is computed using equation (5)
and in equation (5)

$$P = 1 \text{ psi}$$

$$a = 15 \text{ inches}$$

The k_w^1 functional provides a "mathematical equivalent,"^g - based on elastic material constants - to the plate bearing test from which k is

^g "mathematical equivalent" is somewhat loosely used here. Refer to Section III for a discussion of this point.



Idealizations for k_s^1 equivalency where the horizontal stress at B for both idealizations is equal.

Figure 4. Usage of Westergaard stress functional.

derived. Equations (5 and 6) imply that k_w^1 is only a function of the system material parameters $[E_2, \nu_2, h_2 \dots \nu_N]$ and is independent of aircraft loading.

k_w^2 and k_s^1 functionals. These functionals are derived in a two step operation (Figures 3b and 4). One of the steps consists of computing δ and σ for the Westergaard idealization (i.e., the pavement's peak displacement and maximum tensile stress). Equations (1 and 2) are only a first order approximation to the "exact" calculation of δ and σ , and are usually of acceptable accuracy. However, in development of the functionals it is desirable that accurate (i.e., "exact") solutions of the Westergaard idealization be computed for whatever system parameters are employed. The basis for these "exact" solutions and a discussion of their merits is presented in Appendix B. It is the "exact" form of equations (1 and 2) that is used to develop the k_w^2 and k_s^1 functionals.

k_w^2 and k_s^1 are more like algorithms, rather than actual mathematical expressions, and are computed by iteration. For the first step, the solution of the elastic layer equations (2 and 4) is computed where "P" is the tire pressure, "a" is the tire radius, and the other constants are derived from the system parameters: E, ν , and h. During the second step, various "guessed" values for k are substituted in the "exact" form of the Westergaard equations (1 and 3). By requiring that the values for δ of the second step equal the δ of the first step, a value of k is computed, which is denoted as k_w^2 . The equivalent k, computed by matching the two σ , is k_s^1 . The functionals k_w^2 and k_s^1 are dependent on both the system material parameters and the aircraft loading.

2. ELAST Computer Program

All three functionals $[k_w^1, k_w^2, \text{ and } k_s^1]$ are computed by the ELAST computer program described in Appendix C. Two additional functionals are also computed by ELAST: k_w^3 and k_s^2 . As mentioned earlier, the usage

of equations (1 and 2) for computation of k_w^2 and k_s^1 is felt to be inappropriate. However, this decision makes it awkward to use either the k derived from k_w^2 in equation (1), or the k derived from k_s^1 in equation (2). Thus, in a manner analogous to the derivation of k_w^2 and k_s^1 , k_w^3 and k_s^2 are derived, using equations (1 and 2), instead of the "exact" expressions in Appendix B. The consequences of this dual derivation are shown in the next section.

3. Usage of Westergaard Functionals

Five different functionals have been introduced. The basis for these functionals is summarized below.

1. k_w^1 provides a k which is based on the simulation of a plate bearing test using an elastic layer idealization.
2. k_w^2 provides a k which is based on the requirement that the deflections computed from equation (3), and the "exact" form of equation (1), be equal.
3. k_w^3 is similar to k_w^2 , except that equation (1) is used instead of its "exact" form.
4. k_s^1 provides a k which is based on the requirement that the stress computed from equation (4), and the "exact" form of equation (2), be equal.
5. k_s^2 is similar to k_s^1 , except that equation (2) is used instead of its "exact" form.

There is a fundamental difference between k_w^1 and k_w^2 , k_w^3 , k_s^1 , and k_s^2 . k_w^1 provides an equivalency between the elastic layer and Westergaard subgrade stiffness, which is not based on any Westergaard formulae or an aircraft loading. In contrast, the other functionals are derived from a specific Westergaard equation and tire load.

Examples illustrating the functionals' usage. A number of pavement sections were selected to illustrate the usage of the functionals. These sections are shown in Figure 5, and represent the widest possible variation of rigid pavement types for which sufficient materials data was available. The sections shown are roughly divided into three basic types according to the value of k . The "A" type is generally a concrete cap placed on a granular material with a k from 300-500 pci. The "B" type pavement is generally a concrete cap placed on a silt, or clayey material, with a k of 50-200 pci. "A" and "B" represent classic applications for the Westergaard idealization: a relatively thin, stiff, "plate like" layer over a relatively soft, homogeneous subgrade. The "C" type pavement is somewhat hodgepodge, but includes mostly stabilized sections of various depths and k values.

For the sections of Figure 5, Tables 1 and 2 list the computed values for the five functionals and the measured values of modulus k . Also shown are the " δ " and " σ " computed from the Westergaard equations (1) and (2), respectively; two sets of values were computed by employing both k and k_w^1 . In addition, " δ " and " σ " for the elastic layer idealization also appear. For Table 1, the values of displacement and stress, as well as functionals [k_w^2 , k_w^3 , k_s^1 , and k_s^2], result from a 30,000 pound load applied over a 30-inch-diameter circle. While for Table 2, a 27,000 pound load, over a 11.4-inch-diameter circle, is used.

Usage of k_w^1 . As mentioned, k_w^1 is the elastic layer equivalent to the modulus of subgrade reaction. There are two significant ways in which k_w^1 can be utilized.

First, k_w^1 , offers a means to unite the two most widely available characterizations of the soil's response to load. For the sections of Figure 5, the mean percent difference of k_w^1 , with respect to k , is shown at the top of Table 3. The asterisks in Table 1 indicate those sections where k_w^1 is within 25% of k (i.e., 6 out of 20), and the asterisks in Table 2 indicate those sections where k is greater than k_w^1 (i.e., 5 out of 20). While the disparity between k_w^1 and k is

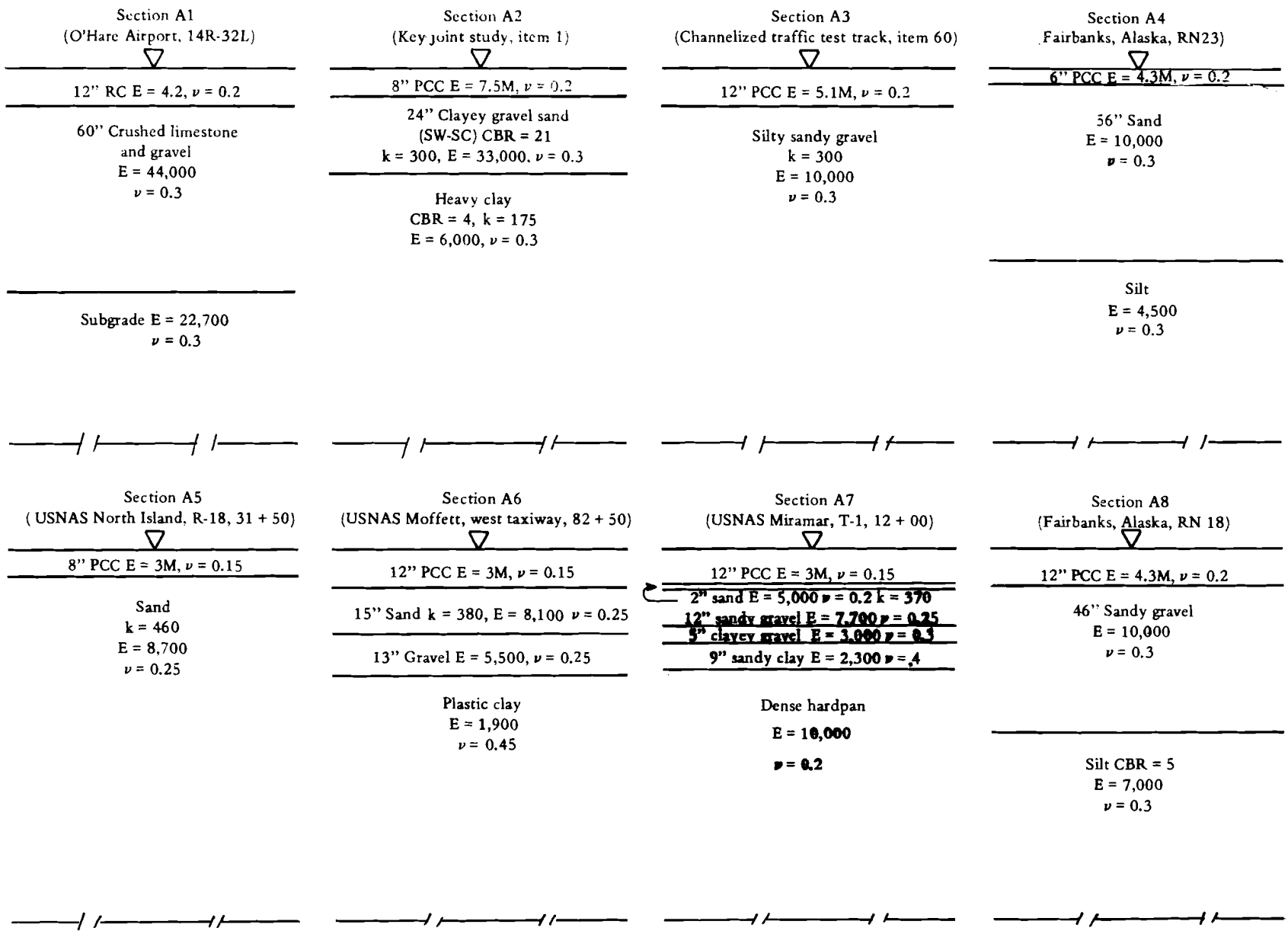
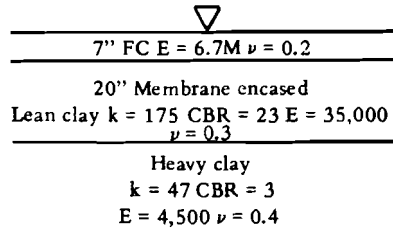
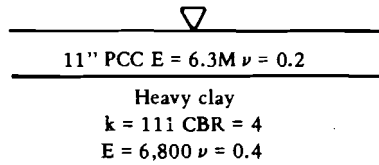


Figure 5. Pavement sections.

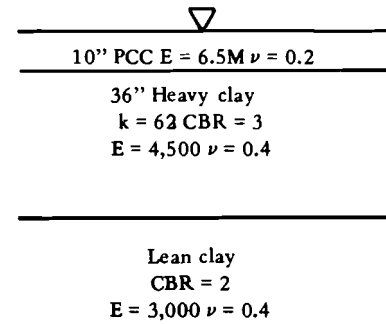
Section B1
Soil stabilization pavement study, item 1



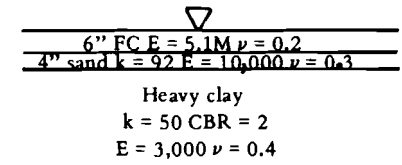
Section B2
Key joint study, item 2



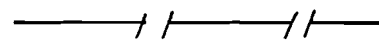
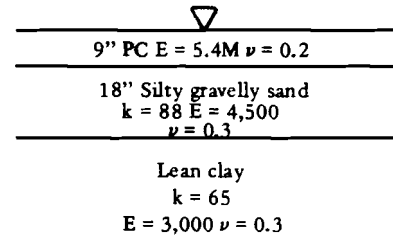
Section B3
MWHGL, item 1



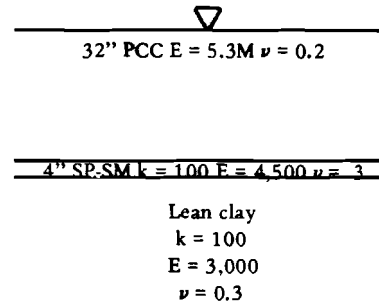
Section B4
Key joint study, item 5



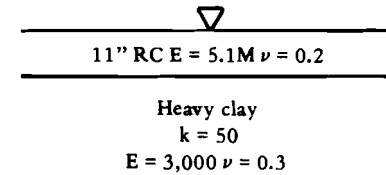
Section B5
Sharonville prestressed concrete track, P1



Section B6
Sharonville, track A, item 71



Section B7
Channelized traffic test track, item 51



RC Reinforced concrete
PCC Portland cement concrete
PC Prestressed concrete
FC Fibrous concrete
LC Lightweight concrete



Figure 5. continued

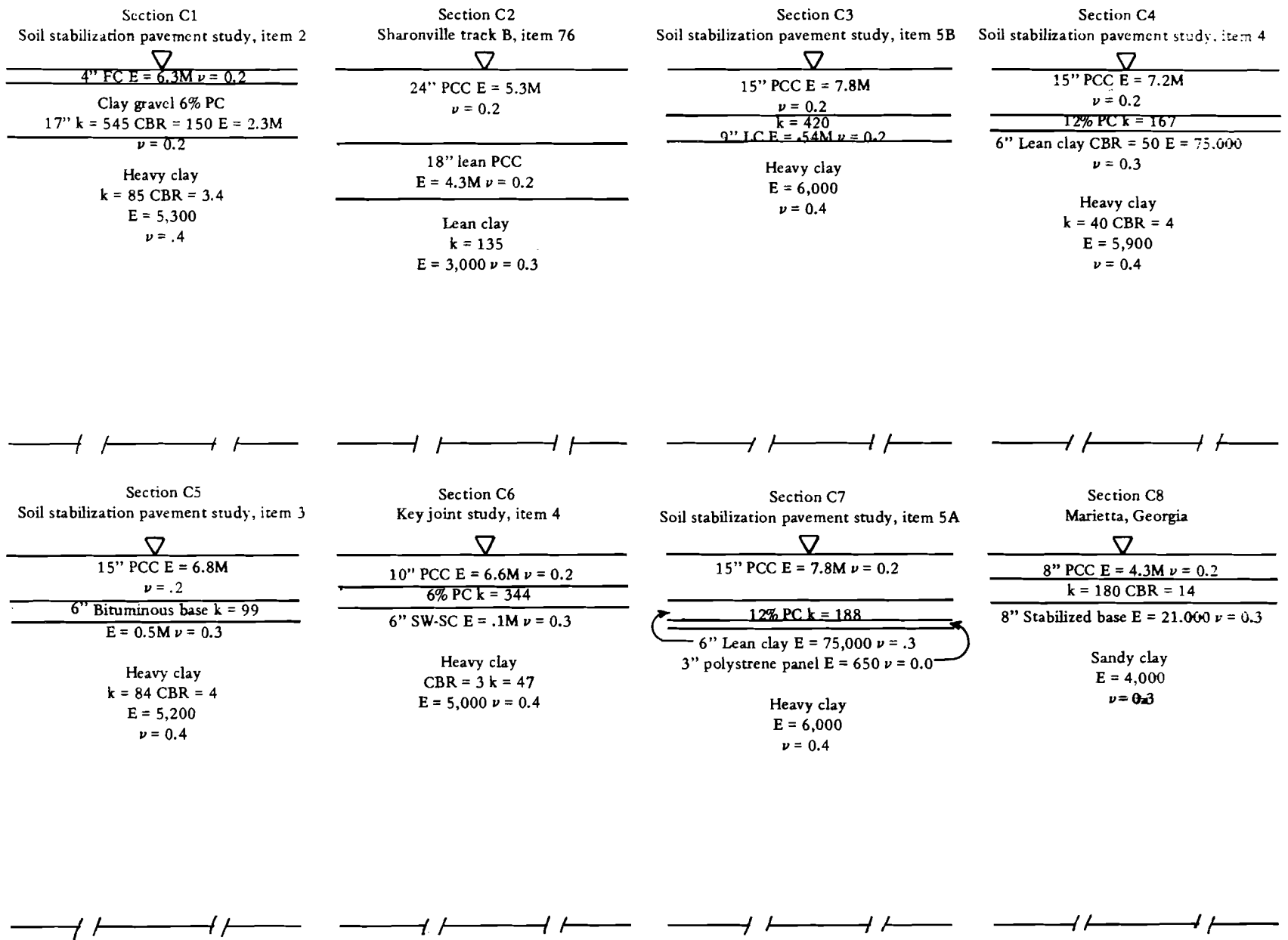


Figure 5. continued

Table 1. Results of Usage of Westergaard Functionals^a

Section Number	Westergaard Constant and Functionals						Elastic Layer Response	
	$k/\sigma^b/\delta^c$ PCI/PSI/in.	$k_w^1/\sigma^b/\delta^c$ PCI/PSI/in.	k_w^2 PCI	k_w^3 PCI	k_s^1 PCI	k_s^2 PCI	δ^e in.	d^f PSI
A1	N.A. ^d	1,424/138/0.004	257	239	1,201	965	0.009	149
A2	300/371/0.011	535/333/0.008	49	48	308	265	0.029	380
A3* ^g	300/190/0.007	366/184/0.007	53	51	147	121	0.018	217
A4	N.A.	310/487/0.021	62	61	255	212	0.050	532
A5	460/270/0.013	309/295/0.017	80	77	226	194	0.035	325
A6	380/160/0.008	149/187/0.014	8	8	33	28	0.063	235
A7	370/161/0.009	212/177/0.011	48	46	105	88	0.025	202
A8	N.A.	339/181/0.008	39	38	130	107	0.023	216
B1	175/487/0.019	414/411/0.012	40	39	287	246	0.041	457
B2	111/260/0.013	270/228/0.008	32	31	84	70	0.024	276
B3	62/328/0.019	158/288/0.011	12	12	35	31	0.045	359
B4	92/653/0.037	122/618/0.032	22	21	59	52	0.080	720
B5	88/360/0.021	136/338/0.016	14	14	41	36	0.053	408
B6*	100/43/0.003	110/42/0.003	4	4	10	12	0.016	53
B7	50/280/0.021	110/252/0.014	11	11	30	25	0.046	305
C1	545/720/0.022	1,615/429/0.011	698	692	N.P. ⁱ	N.P.	0.019	62
C2* ^h	135/25/0.002	110/27/0.002	3	3	8	15	0.013	32
C3	420/136/0.004	1,263/115/0.002	42	40	140,000	92,000	0.012	33
C4	167/152/0.006	309/140/0.005	19	19	65	51	0.019	175
C5	99/161/0.008	408/134/0.004	18	18	206	162	0.020	152
C6*	344/255/0.008	282/264/0.009	24	24	105	90	0.031	312
C7*	188/151/0.006	194/151/0.005	17	17	47	37	0.019	182
C8*	180/368/0.019	205/360/0.017	27	26	96	84	0.051	419

^a A 30,000 lb load applied over a 30-inch-diameter circular area was used in computation of k_w^2 , k_w^3 , k_s^1 , k_s^2 , δ , and σ .

^b Stresses are at bottom of first layer centered under load and are computed using equation (2).

^c Displacements are on surface centered under the load and are computed using equation (1).

^d The "k" parameter was not available for these sites.

^e Displacements are on surface centered under the load and are computed using equation (3).

^f Stresses are at bottom of first layer centered under load and are computed using equation (4).

^g Asterisk denotes sections where k_w^1 is within 25% of k.

^h The top two layers of this section were combined to form a "pseudo" top layer.

ⁱ Not permissible; compressive stress at the bottom of the first layer.

Table 2. Results of Usage of Westergaard Functionals for F4 Load^a

Section Number	Westergaard Constant and Functionals						Elastic Layer Response	
	$k/\sigma^b/\delta^c$ PCI/PSI/in.	$k_w^1/\sigma^b/\delta^c$ PCI/PSI/in.	k_w^2 PCI	k_w^3 PCI	k_s^1 PCI	k_s^2 PCI	δ^e in.	σ^f PSI
A1	N.A. ^d	1,424/228/0.0035	262	221	1,385	1,600	0.0089	225
A2	300/569/0.010	535/534/0.0078	49	48	347	275	0.0267	575
A3	300/275/0.007	366/270/0.0063	52	49	157	168	0.0174	291
A4	N.A.	310/855/0.0208	63	61	279	217	0.0477	894
A5* ^g	460/468/0.013	309/491/0.0164	81	75	243	196	0.0337	517
A6*	380/244/0.008	149/268/0.0131	8	8	35	38	0.0578	303
A7*	370/244/0.008	212/259/0.0108	48	44	111	122	0.0241	274
A8	N.A.	339/268/0.0072	39	37	139	150	0.0219	289
B1	175/745/0.018	414/677/0.0115	40	39	340	262	0.0380	714
B2	111/358/0.012	270/330/0.0076	32	32	86	84	0.0225	367
B3	62/446/0.018	158/410/0.0113	13	12	35	32	0.0410	472
B4	92/1,005/0.035	122/974/0.0307	22	21	62	48	0.0744	1,074
B5	88/510/0.020	136/489/0.0155	14	14	43	34	0.0489	555
B6	100/54/0.003	110/54/0.0026	3	4	9	178	0.0144	52
B7	50/377/0.019	110/352/0.0132	12	11	29	30	0.0420	393
C1	545/1,587/0.023	1,615/1,324/0.0132	987	929	5,266,000	350,000	0.0176	21
C2* ^h	135/32/0.002	110/33/0.0020	3	3	5	466	0.0121	30
C3	420/189/0.003	1,263/170/0.0020	45	40	648,000	2,302,000	0.0111	41
C4	167/204/0.006	309/193/0.0042	21	18	65	116	0.0172	210
C5	99/212/0.008	408/187/0.0037	20	17	337	564	0.0183	182
C6*	344/380/0.008	282/388/0.0083	25	24	129	115	0.0288	422
C7	188/203/0.005	194/203/0.0050	18	16	47	83	0.0177	217
C8	180/566/0.018	205/559/0.0168	27	26	107	84	0.0478	612

- ^a a 27,000 lb load applied over a 11.4-inch-diameter circular area (approximation of a single tire load from a F4 Phantom II fighter aircraft) was used in computation of k_w^2 , k_w^3 , k_s^1 , δ , and σ .
- ^b Stresses are at bottom of first layer centered under the load and are computed using equation (2).
- ^c Displacements are on surface centered under the load and are computed using equation (1).
- ^d The "k" parameter was not available for these sites.
- ^e Displacements are on surface under the load and are computed using equation (3).
- ^f Stresses are at bottom of first layer centered under the load and are computed using equation (4).
- ^g Asterisk denotes sections where k is greater than k_w^1 .
- ^h The top two layers of this section were combined to form a "pseudo" top layer.

Table 3. Accuracy Measures Associated With k_w^1 .

	For values taken from	"A" type pavements	"B" type pavements	"C" type pavements
1. Mean % difference of k_w^1 with respect to k , followed by its standard deviation	Table 1 or Table 2	47%, ±22%	93%, ±58%	86%, ±110%
2. Mean % difference of σ^d (computed from k_w^1) with respect to σ^d (computed from k), followed by its standard deviation	Table 1 Table 2	9%, ±5% 8%, ±6%	9%, ±5% 6%, ±3%	9%, ±14% 5%, ±6%
3. Mean % difference of δ^c (computed from k_w^1) with respect to δ^c (computed from k), followed by its standard deviation	Table 1 Table 2	31%, ±27% 37%, ±22%	27%, ±15% 27%, ±11%	23%, ±18% 17%, ±21%
4. Mean % difference of σ^d (computed from k_w^1) with respect to σ^b (elastic layer), followed by its standard deviation	Table 1 Table 2	11%, ±4% 7%, ±3%	16%, ±4% 10%, ±3%	13%, ^c ±6% 9%, ^e ±5%
5. Mean % difference of δ^c (computed from k_w^1) with respect to δ^d (elastic layer), followed by its standard deviation. Note: Westergaard deflections are always less than those of elastic layer	Table 1 Table 2	63%, ±8% 62%, ±11%	70%, ±7% 69%, ±7%	75%, ±6% 65%, ±28%

^a σ is defined in footnote *b*, Table 1.

^b σ is defined in footnote *f*, Table 1.

^c δ is defined in footnote *e*, Table 1.

^d δ is defined in footnote *e*, Table 1.

^e The contribution of sections C1 and C3 were omitted from this percentage because of their extreme differences from the other percentages.

often large, the corresponding disparities between values of σ are quite small (Table 3, second entry). On the other hand, δ is more highly influenced (Table 3, third entry).

The second important application for k_w^1 provides a direct comparison of the Westergaard and elastic layer idealizations, and is shown in the last two entries of Table 3. Here, the Westergaard σ and δ are calculated using k_w^1 , which gives the Westergaard subgrade approximately the same vertical stiffness as the elastic layer subgrade. This application of k_w^1 demonstrates that the two idealizations provide relatively similar values for σ , except in rather special situations, such as, section C3. The effect of the differences between the idealizations is illustrated by the consistently larger displacement prediction produced by the elastic layer analysis.

Usage of k_w^1 indicates that, at least for the sections of Figure 5:

1. σ can be computed from equations (2 or 4) using quantities E and ν , k , or k_w^1 , with relatively little change in results.
2. In some sections under certain loading conditions (e.g., C3), the shear transfer between the top layers is of significant importance. For some of these cases where no "clear cut" boundary exists between pavement and subgrade, utilization of the Westergaard idealization is not appropriate. In other cases, stress computations using the Westergaard idealization are complicated by the need to define a "pseudo" top layer stiffness and the resulting necessity to back calculate the layer stresses from those of the "pseudo" layer.
3. When k_w^1 is used to force the match of Westergaard subgrade stiffness to that of elastic layer, there is a relatively constant difference in predicted displacement - approximately 70% less deflection is computed by Westergaard. This appears to be caused by the differences between a fluid and an elasticity subgrade.

Usage of k_w^2 , k_w^3 , k_s^1 , and k_s^2 . These functionals provide another means of comparing the Westergaard and the elastic layer idealizations. For example, if the value of k_s^2 is substituted for k in equation (2) then the resulting stress will equal the σ computed from the elastic layer idealization. Thus, for section A2 of Table 1, a value of ($k = 265$) would be needed in Equation (2) to produce the 380 psi elastic layer stress - by comparison ($k_w^1 = 535$) and ($k = 300$). This implies that given the elastic layer stress and given equation (2), then the modulus of subgrade reaction is 265 instead of either 535 or 300. Essentially, k_s^2 offers a direct comparison between the two idealizations that is unfettered by the requirement to simulate a plate bearing test, which is associated with the employment of k_w^1 . k_s^1 is similar to k_s^2 except that the "exact" form of equation (2) is used (see Appendix B).

Functionals k_w^2 and k_w^3 are analogous to k_s^1 and k_s^2 where displacements, rather than stresses, are involved. Thus, for section A2 of Table 1, a value of ($k = 48$) would be needed in equation (1) to produce the 0.029 inches of elastic layer deflection - by comparison ($k_w^1 = 535$) and ($k = 300$). The "k" values given by k_w^2 or k_w^3 are markedly lower than those measured, or computed using k_w^1 . This qualitatively supports the findings which resulted from utilizing functional k_w^1 , that is, of the two idealizations, the Westergaard one consistently predicts a smaller δ .

The following are the significant results associated with these four functionals. These results are based on the responses shown in Tables 1 and 2.

1. A consistent 88% difference (standard deviation, 16%) exists for k_w^2 with respect to k_w^1 . Thus, δ of an elastic layer solution can be roughly computed from equation (1) by reducing k by 90%.
2. Values of k_s^1 usually occur rather randomly between 3% and 93% of k_w^1 . When the value of k_s^1 exceeds k_w^1 , it is an indication that the Westergaard idealization is inapplicable. Often combining the upper stiff layers into a "pseudo" top layer removes

the problem. This is done for the top two layers of section C2.

3. Through a comparison of k_w^1 to k_s^2 and k_w^2 to k_w^3 , the consequences of including the effects of inplane and shear stresses in the top layer [i.e., "exact" equations versus equations (1 and 2)] generally appear negligible. In only a few instances, where k_s^2 is much larger than k_s^1 , are these effects noticeable. However, in these cases - while other response quantities may be affected - the ones shown in Tables 1 and 2 are not.

III. SUMMARY

In summary, the functionals demonstrate that the problem of correlating the Westergaard and elastic layer predictions of σ and δ is primarily related to inconsistencies in material characterization. With respect to inconsistencies in mathematical idealization, the following statements are appropriate.

1. Given that the difference between k_w^1 and k is less than 100%, σ appears unaffected by the idealization except in relatively rare circumstances where Westergaard idealization does not work (e.g., C-1 and C-3).
2. For the computation of δ , the disparities caused by idealization can be filtered out. That is, δ predicted by the elastic layer idealization is roughly 70% greater than that predicted by Westergaard equation (1). To approximately predict an elastic layer δ using equation (1) reduce k by 90%.

The disparity between k and k_w^1 is difficult to interpret. It is largely a comparison of one material characterization to another, i.e., k versus E and ν . With respect to the objectives of this report, the most significant question is: should k compare with k_w^1 . A corollary

question of a more general nature is also significant: can satisfactory responses be predicted using linear, homogeneous, layered approximations of soil materials. Although neither question can be given a blanket answer, some general comments follow.

1. k versus k_w^1 .

Matching k_w^1 to k . Both Westergaard and elastic layer theories are predicated on the "basic assumption" that the pavement system is divisible into homogeneous layers whose materials have linear, homogeneous responses to aircraft loads. This statement implies that k is mathematically equivalent to k_w^1 given that the boundary value problem solved in Appendix A^h is a satisfactory approximation of a plate bearing testⁱ. In other words - given accurately measured values of k , E , and ν and belief in the "basic assumption" - if a pressure load P of radius 15 inches is applied to an elastic layer approximation of the subgrade, the predicted and measured responses must be similar.

^h i.e., a uniform circular pressure applied to a layer system.

ⁱ While a plate test is reasonably approximated by this boundary value problem, it is not exactly so, and other boundary value problems which were deemed less appropriate, might also be used (such as, uniform circular displacement). Also considered was the incorporation of the effects of the plate load hardware into the mathematics associated with the k_w^1 functional. However, because consideration of these effects produce complications - both in the functional's mathematical formulation and its usage - for rather dubious benefits (given the constraints of linear theory), and because of the variability of hardware configurations, this incorporation appears both unwarranted and inconsistent with one of the functional's purposes (i.e., simplicity). Therefore, any consideration of plate hardware is omitted.

Tables 1 and 2 aptly demonstrate that the values of k and k_w^1 may disagree. Given that k_w^1 should equal k , these discrepancies most likely indicate that E and ν values are incorrect; in that, k is a direct measure of insitu response garnered from a testing procedure that is relatively easy to accomplish, while E and ν are usually either estimated or measured with rather rudimentary equipment and procedures.

At this point, at least heuristically, it must be demonstrated that matching k to k_w^1 is a desirable goal. Certainly, σ seems "unconcerned," but getting the δ predictions to correlate between the two methods depends directly on this matching. Secondly, while the relationship of simulating a plate test to a live load prediction is not "one-to-one,"^j k does represent the most widely available parameter measuring insitu conditions. To ignore matching it, would require solid contrary data. Finally, matching k to k_w^1 provides an intuitive "feel" for the elasticity idealization, which is missing in a "straight" elasticity solution. Thus, it would seem that, at least as a "base line," matching k_w^1 to k is a worthwhile goal.

Selection of E and ν . Because of the complexities associated with E and ν , their direct selection based on laboratory and/or field tests is suspect.^k Probably the most satisfactory means for utilizing the

^j Matching k does not imply that the elasticity material parameters can not change radically under aircraft loading. For example, under the level and distribution of loading associated with large aircraft, the soil stiffness could be considerably stronger or weaker than that associated with getting k_w^1 to match k .

^k Not only are the parameters difficult to determine per se, but their influence on the idealization - and thus, the consequences of their erroneous selection - is hard to follow. In determining these parameters, probably the most difficult element to assess is the impact of the insitu conditions. Often laboratory or estimated values of E and ν are employed as though the insitu conditions didn't exist. For a large part of the subgrade, the live load effects on E and ν are negligible compared to the influence of such insitu parameters as: gravity and pre-consolidation stresses, saturation, void ratio, etc. For example, at depths greater than 2-3 feet within the subgrade, gravitational stresses are often greater than those produced by the aircraft.

large variety of data that influences these quantities is employment of material models⁷. These mathematical entities coalesce the various laboratory (e.g., triaxial test) and field data (e.g., void ratio, saturation) into a single coordinated representation of a material. The model is used to calculate appropriate linear constants (E and ν) as functions of the insitu conditions, as well as either the estimated or computed live load stresses.

Effects of Material Linearity. The following three points, while not very specific, provide a "flavor" of the effect associated with making the material parameters linear. As used in linear analysis, k and E and ν are linear approximations of two separate types of phenomena. k involves what is essentially a one dimensional characterization of a large, insitu soil mass; relatively large loads are added to whatever insitu loads exist, and the results are biased by the soil nearer the load. E and ν provide a two dimensional characterization of a small (probably distributed, certainly not insitu) soil sample under probably higher stress levels. To measure E and ν accurately requires elaborate hardware and test procedures. To measure E alone (and estimate ν), is still a complicated procedure when compared to measuring k . In addition, k is derived from a test which inherently forces the soil into a nonlinear, inhomogeneous response. While E and ν - computed from a triaxial test - are nonlinear phenomena, their measurement does not create an inhomogeneous situation. The significant points are: that the k parameter represents linearization of both stiffness and layer inhomogeneity while E and ν only linearize stiffness, that these two types of parameters are generally collected from two different stress ranges, and that one is a gross behavior for a small portion of the subgrade while the other

⁷ Reference (5) provides an expanded discussion of material models. These same types of models are used in nonlinear analyses albeit more directly.

measures macroscopic behavior and is applicable at any point in the soil mass.

As a demonstration of the effects of linearization, equation (6) is used to compute a variety of k_w^1 based on varying the plate radius "a" (i.e., k_w^1 is computed for "a" = 7.5, 30, 300, and 3,000 inches). For the "A" type sections of Figure 5, k_w^1 is roughly proportional to the reciprocal of "a". This behavior does not match the "conventional wisdom" associated with field results, where utilizing plates over 30-inch-diameter results in little change of k.

Certainly, linear theories are of benefit to pavement analysts, but employing them to check themselves is seemingly an impossible task. In order to establish the limits of their employment it is necessary to check them against a high precision idealization [e.g., the WINDAX computer code mentioned in Reference (5)]. In turn, this precise model must base its verification on a few precise field tests.

Summary. In summary, k and k_w^1 is expected to agree, given appropriate values of E and ν . This agreement is of "base line" importance for those pavement systems where the inhomogeneities caused by the plate load test within a material layer are of minimal importance.

Tables 1 and 2, while apt for demonstration, are based on data which is insufficiently accurate - especially the values for E and ν - to warrant any categorical conclusions concerning the relationship of k and k_w^1 . Data of higher quality is needed to accurately validate the applicability of this functional.

2. Derivation of E from k

All of the functionals depend on deriving a "k" from the elastic layer parameters E, ν , and h. Theoretically, because only linear equations and assumptions are involved, the reverse is possible - that is, computation of some or all of the elasticity parameters from various values of k. Practically speaking, this approach has significant flaws,

in that, the variety of k values needed is usually not available and that the basically one dimensional nature of k does not easily extend itself to the two dimensional nature of elasticity. However, to a limited extent and in simple circumstances some of this "reverse" computation is relevant.

3. Basic Assumption Versus the Real World

The developments presented in this report are predicated on the "basic assumption" - pavements are composed of homogeneous layers whose materials remain homogeneous and linear under aircraft loads. There is enough evidence [e.g., Reference (5)] to support the conclusion that flexible pavements do not abide by the "basic assumption." For rigid pavements a significant lack of data has hindered such conclusions, although some tests (5) of rigid pavements on substandard subgrades significantly deviate from linear theory.

Moreover, if σ is the only design criterion, the impact of one idealization versus another, or "basic assumption" versus the "real world" is blunted. To a lesser extent, this is also true of δ . However, future design procedures will rely on more extensive criteria, for example, maximum shear strains within each subgrade layer. The prediction of criteria, such as these, is more sensitive to material characterization and certainly requires procedures more sophisticated than Westergaard and also probably more sophisticated than elastic layer.

IV. CONCLUSIONS AND RECOMMENDATIONS

The data presented in this report leads to the following conclusions. These conclusions are predicated on the sections shown in Figure 5 and are made within the context of linear analysis. Without further validation, it is unreasonable to assume - for either sections dissimilar to those shown or for loadings significantly different from those used to generate Tables 1 and 2 - that these conclusions are appropriate.

1. Computation of peak tensile stress in the concrete layer is relatively insensitive to the subgrade material properties. For a reasonable set of material values this stress can be expected to vary by only 10%.
2. The Westergaard idealization consistently under predicts the peak deformation computed by an elastic layer system. For the sections shown in Figure 5, this disparity is roughly 70%. To approximately compute the elastic layer deformation using a Westergaard idealization, reduce k by 90%.
3. If k_s^1 is greater than k_w^1 , then the Westergaard idealization is inapplicable (see Section II.3 for the definition of k_s^1 and k_w^1).
4. Comparing k with k_w^1 , provides a measure of the accuracy with which the material parameters of the elastic layer system were chosen. Comparisons with k involving the other functionals is not consistent, in that these functionals, unlike k , are dependent on the top layer's material parameters and the aircraft loading.
5. The applicability of both the Westergaard and elastic layer idealizations in predicting design criteria, other than peak stress and deflection, is questionable.
6. Equations (1 and 2) are of sufficient accuracy to solve the Westergaard idealization.

The following recommendations appear warranted based on the data presented in this report.

1. Utilize the ELAST computer program, described in Appendix C, to compute a rigid pavement's peak stress and displacement. These responses are computed by both the elastic layer and Westergaard methods of analysis. Additionally, ELAST computes several quantities, denoted as functionals, which provide a "bridge"

between the predictions of these two methods. These quantities are intended to assist the engineer in deciding on the applicability of one method versus another.

2. Conduct tests of a series of rigid pavement systems. This series shall be designed to test the "basic assumptions" and peak deflection predictions of the Westergaard and elastic layer theories, and to establish the validity of the k_w^1 functional. Important components of these tests are accurate measure of all material parameters (i.e., E, ν , and k); close control of material placement and preparation; test sections that are specifically designed to validate analytical theories; and comprehensive and accurate measure of the pavement section's response to large (over 80 kips) axisymmetric loads.
3. Based on these tests, establish the need for more precise determination of the material parameters E and ν for use in conjunction with the k_w^1 functional and elastic layer analysis. If necessary, material models should be developed to provide more effective use of the data associated with the selection of E and ν . It is especially important to have a means for incorporating the gravitational effects into their determination.
4. Various finite element idealizations should be compared with those of both elastic layer and Westergaard to determine limitations of the simpler theories. This, however, can only be accomplished using test data of a higher quality than is presently available.

Appendix A

MATHEMATICAL DESCRIPTION FOR THE MULTILAYER ELASTIC PROBLEM

The multilayer elastic problem consists of N layers of homogeneous linear elastic material of infinite lateral extent (Figure A-1). The layers are numbered from top to bottom. Each layer (n) has a Young's modulus (E_n), a Poisson's ratio (ν_n), and a thickness (h_n : except for the Nth layer which has an infinite depth). A uniform pressure (P) is applied over a circular area of radius (a) to the top surface of the top layer. The problem is to find the downward displacement [$w(0,0)$] at T and the lateral stress [$\sigma_{rr}(0,h_1)$] at B, where T is the origin of a cylindrical coordinate system (R,Z). The Z coordinate is positive downward, and for this problem the spatial coordinate r will always be zero. The layers are taken to be bonded at their interfaces.

Because the problem is axial symmetric, it is governed by a single stress function (ϕ) and the following differential equations [Reference 6].

$$\nabla^4 \phi = 0 \quad (\text{A-1})$$

$$\sigma_{rr} = \frac{\partial}{\partial z} \left(\nu \nabla^2 \phi - \frac{\partial^2 \phi}{\partial r^2} \right) \quad (\text{A-2})$$

$$\sigma_{zz} = \frac{\partial}{\partial z} \left[(2-\nu) \nabla^2 \phi - \frac{\partial^2 \phi}{\partial z^2} \right] \quad (\text{A-3})$$

$$\sigma_{rz} = \frac{\partial}{\partial r} \left[(1-\nu) \nabla^2 \phi - \frac{\partial^2 \phi}{\partial z^2} \right] \quad (\text{A-4})$$

$$w = \frac{1+\nu}{E} \left[2(1-\nu) \nabla^2 \phi - \frac{\partial^2 \phi}{\partial z^2} \right] \quad (\text{A-5})$$

$$u = - \left[\frac{1+\nu}{E} \frac{\partial^2 \phi}{\partial r \partial z} \right] \quad (\text{A-6})$$

where
$$\nabla^2 = \frac{\partial^2}{\partial r^2} + \frac{1}{r} \frac{\partial}{\partial r} + \frac{\partial^2}{\partial z^2} \quad (\text{A-7})$$

$$\sigma_{rr} = \text{radial stress}$$

$$\sigma_{zz} = \text{vertical stress}$$

$$\sigma_{rz} = \text{shear stress}$$

$$w = \text{vertical displacement}$$

$$u = \text{horizontal displacement}$$

The above equations are applicable for each layer.

The boundary conditions at the layer interfaces (assumed bonded) are:

$$\sigma_{zz}^n(r, H_n) = \sigma_{zz}^{n+1}(r, H_n) \quad (\text{A-8})$$

$$\sigma_{rz}^n(r, H_n) = \sigma_{rz}^{n+1}(r, H_n) \quad (\text{A-9})$$

$$w^n(r, H_n) = w^{n+1}(r, H_n) \quad (\text{A-10})$$

$$u^n(r, H_n) = u^{n+1}(r, H_n) \quad (\text{A-11})$$

where
$$H_n = \sum_{i=1}^n h_i$$

and n and n+1 are indices of adjacent layers. The boundary conditions at the top are:

$$\sigma_{zz}(r, 0) = \begin{cases} -P & \text{for } 0 < r < a \\ 0 & \text{for } r > a \end{cases} \quad (\text{A-12})$$

$$\sigma_{rz}(r, 0) = 0 \quad (\text{A-13})$$

The general solution employed for the basic differential equation (A-1) contains four constants for each layer. The other differential equations (A-2 to A-6) and the boundary conditions (A-8 to A-13) are employed to determine these arbitrary constants.

To provide a tractable solution method, Hankel transforms $[L_0, L_1]$ are employed.

$$L_0(\phi) = \bar{\phi} = \int_0^{\infty} r \phi J_0(pr) dr$$

where J_0 is a zeroth order Bessel function of the first kind
 $\bar{\phi}$ is $L_0(\phi)$ where the bar denotes a transformed variable
 p is the transform parameter

$$L_1\left(\frac{\partial g}{\partial r}\right) = \int_0^{\infty} \frac{\partial g}{\partial r} r J_1(pr) dr$$

where g is any arbitrary function of r and z

J_1 is a Bessel function of the first kind, first order

Use of these transformations change the problem from the r, z space to the p, z space which changes the partial differential form of equations (A-1 to A-7) to that of ordinary ones [Reference 7].

$$\text{Thus for } \nabla^2 \phi = \frac{\partial^2 \phi}{\partial r^2} + \frac{1}{r} \frac{\partial \phi}{\partial r} + \frac{\partial^2 \phi}{\partial z^2} \quad (\text{A-14})$$

use of the L_0 Hankel transform results in

$$\begin{aligned} L_0(\nabla^2 \phi) &= \int_0^{\infty} r \nabla^2 \phi J_0(pr) dr = \int_0^{\infty} r \frac{\partial^2 \phi}{\partial r^2} J_0(pr) dr + \\ &\int_0^{\infty} \frac{\partial \phi}{\partial r} J_0(pr) dr + \int_0^{\infty} r \frac{\partial^2 \phi}{\partial z^2} J_0(pr) dr \end{aligned}$$

$$\begin{aligned}
&= r \frac{\partial \phi}{\partial r} J_0(pr) \Big|_{r=0}^{\infty} - \int_0^{\infty} \frac{\partial \phi}{\partial r} \frac{\partial}{\partial r} [r J_0(pr)] dr + \\
&\int_0^{\infty} \frac{\partial \phi}{\partial r} J_0(pr) dr + \int_0^{\infty} r \frac{\partial^2 \phi}{\partial z^2} J_0(pr) dr
\end{aligned}$$

It is assumed that the function ϕ is such that the top limit of the first term goes to 0, so

$$\begin{aligned}
L_0 (V^2 \phi) &= - \int_0^{\infty} \frac{\partial \phi}{\partial r} J_0(pr) dr + \int_0^{\infty} pr \frac{\partial \phi}{\partial r} J_1(pr) dr \\
&+ \int_0^{\infty} \frac{\partial \phi}{\partial r} J_0(pr) dr + \int_0^{\infty} r \frac{\partial^2 \phi}{\partial z^2} J_0(pr) dr \\
&= \int_0^{\infty} pr \frac{\partial \phi}{\partial r} J_1(pr) dr + \frac{\partial^2}{\partial z^2} \int_0^{\infty} r \phi J_0(pr) dr \\
&= \phi pr J_1(pr) \Big|_{r=0}^{\infty} - \int_0^{\infty} \phi \frac{\partial}{\partial r} [pr J_1(pr)] dr + \frac{\partial^2 \phi}{\partial z^2} \\
&= - \int_0^{\infty} p \phi \frac{\partial}{\partial pr} [pr J_1(pr)] dr + \frac{\partial^2 \phi}{\partial z^2} \\
&= \frac{\partial^2 \phi}{\partial z^2} - \int_0^{\infty} p^2 r \phi J_0(pr) dr
\end{aligned}$$

$$\text{or } L_0 (V^2 \phi) = \frac{\partial^2 \phi}{\partial z^2} - p^2 \phi \tag{A-15}$$

Secondly, using L_1 for any arbitrary function $[g(r,z)]$ the following is true:

$$\begin{aligned}
L_1 \left(\frac{\partial g}{\partial r} \right) &= \int_0^{\infty} \frac{\partial g}{\partial r} r J_1(pr) dr \\
&= gr J_1(pr) \Big|_{r=0}^{\infty} - \int_0^{\infty} g \frac{\partial}{\partial r} [r J_1(pr)] dr \\
&= - \int_0^{\infty} g \frac{\partial}{\partial pr} [pr J_1(pr)] dr = - \int_0^{\infty} g pr J_0(pr) dr
\end{aligned}$$

$$\text{or } L_1 \left(\frac{\partial g}{\partial r} \right) = -p \int_0^{\infty} gr J_0(pr) dr = -p L_0(g) \quad (\text{A-16})$$

Equation (A-1) is now ready to be transformed. Applying equation (A-15) twice to equation (A-1) yields

$$\left[\frac{d^2}{dz^2} - p^2 \right]^2 \bar{\phi} = 0 \quad (\text{A-17})$$

The general solution for this ordinary differential equation is

$$\bar{\phi} = [\alpha_1(p) + \alpha_3(p)z] e^{pz} + [\alpha_2(p) + \alpha_4(p)z] e^{-pz} \quad (\text{A-18})$$

The α are arbitrary constants to be determined by the various boundary conditions and other differential equations. There are four such constants (denoted α^n) for each layer which are constant with respect to the differentiation variable z but vary with transform parameter p . The α are sometimes referred to as the characteristic functions.

To determine the α , the problem is worked from the bottom interface ($z = H_{N-1}$) to the top ($z = 0$). To start, the differential equations (A-3 to A-6) are transformed, then equations (A-8 to A-11) are applied at the interfaces. Upon transformation equations (A-3 to A-6) are:

$$L_0(\sigma_{zz}) = \bar{\sigma}_{zz}(p, z) = (1 - \nu) \frac{d^3 \bar{\phi}}{dz^3} - (2 - \nu) p^2 \frac{d\bar{\phi}}{dz} \quad (\text{A-19})$$

$$L_1(\sigma_{rz}) = \bar{\sigma}_{rz}(p, z) = \nu p \frac{d^2 \bar{\phi}}{dz^2} + p^3 (1 - \nu) \bar{\phi} \quad (\text{A-20})$$

$$L_0(w) = \bar{w}(p, z) = \frac{1 + \nu}{E} \left[(1 - 2\nu) \frac{d^2 \bar{\phi}}{dz^2} - 2(1 - \nu) p^2 \bar{\phi} \right] \quad (\text{A-21})$$

$$L_1(u) = \bar{u}(p, z) = \frac{p(1 + \nu)}{E} \frac{d\bar{\phi}}{dz} \quad (\text{A-22})$$

Equations (A-8 to A-11) are similarly transformed

$$\bar{\sigma}_{zz}^n(p, H_n) = \bar{\sigma}_{zz}^{n+1}(p, H_n) \quad (\text{A-23})$$

$$\bar{\sigma}_{rz}^n(p, H_n) = \bar{\sigma}_{rz}^{n+1}(p, H_n) \quad (\text{A-24})$$

$$\bar{w}^n(p, H_n) = \bar{w}^{n+1}(p, H_n) \quad (\text{A-25})$$

$$\bar{u}^n(p, H_n) = \bar{u}^{n+1}(p, H_n) \quad (\text{A-26})$$

For the nth layer, the transformed stress function and several of its derivatives are:

$$\bar{\phi}(p, z) = \left[\alpha_1^n + \alpha_3^n z \right] e^{pz} + \left[\alpha_2^n + \alpha_4^n z \right] e^{-pz} \quad (\text{A-27})$$

$$\begin{aligned} \frac{d\bar{\phi}}{dz} = & \left[p(\alpha_1^n + \alpha_3^n z) + \alpha_3^n \right] e^{pz} \\ & - \left[p(\alpha_2^n + \alpha_4^n z) - \alpha_4^n \right] e^{-pz} \end{aligned} \quad (\text{A-28})$$

$$\begin{aligned} \frac{d^2 \phi}{dz^2} &= p(p\alpha_3^n z + p\alpha_1^n + 2\alpha_3^n) e^{pz} \\ &+ p(p\alpha_4^n z + p\alpha_2^n - 2\alpha_4^n) e^{-pz} \end{aligned} \quad (\text{A-29})$$

$$\begin{aligned} \frac{d^3 \phi}{dz^3} &= p^2(p\alpha_3^n z + \alpha_1^n p + 3\alpha_3^n) e^{pz} \\ &- p^2(p\alpha_4^n z + p\alpha_2^n - 3\alpha_4^n) e^{-pz} \end{aligned} \quad (\text{A-30})$$

By substitution of equations (A-27 to A-30) into equations (A-19 to A-22) then applying the interface equations (A-23 to A-26), the following interface equations are derived (between layers n and $n+1$).

$$\begin{aligned} &\left[-p \alpha_1^n + \alpha_3^n (1 - pH_n - 2v_n) \right] e^{pH_n} \\ &+ \left[p \alpha_2^n + \alpha_4^n (pH_n - 2v_{n+1}) \right] e^{-pH_n} \\ = &\left[-p \alpha_1^{n+1} + \alpha_3^{n+1} (1 - pH_n - 2v_{n+1}) \right] e^{pH_n} \\ &+ \left[p \alpha_2^{n+1} + \alpha_4^{n+1} (pH_n - 2v_{n+1} + 1) \right] e^{-pH_n} \end{aligned} \quad (\text{A-31a})$$

$$\begin{aligned} &\left[-p\alpha_1^n + \alpha_3^n (2 - pH_n - 4v_n) \right] e^{pH_n} \\ &+ \left[-p \alpha_2^n + \alpha_4^n (4v_n - pH_n - 2) \right] e^{-pH_n} \\ = &\beta_1^n \left[-p \alpha_1^{n+1} + \alpha_3^{n+1} (2 - pH_n - 4v_{n+1}) \right] e^{pH_n} \\ &+ \beta_1^n \left[-p \alpha_2^{n+1} + \alpha_4^{n+1} (4v_{n+1} - pH_n - 2) \right] e^{-pH_n} \end{aligned} \quad (\text{A-31b})$$

$$\begin{aligned}
& \left[p \alpha_1^n + \alpha_3^n (2v_n + pH_n) \right] e^{pH_n} \\
& + \left[p \alpha_2^n + \alpha_4^n (pH_n - 2v_n) \right] e^{-pH_n} \\
= & \left[p \alpha_1^{n+1} + \alpha_3^{n+1} (2v_{n+1} + pH_n) \right] e^{pH_n} \\
& + \left[p \alpha_2^{n+1} + \alpha_4^{n+1} (pH_n - 2v_{n+1}) \right] e^{-pH_n} \tag{A-31c}
\end{aligned}$$

$$\begin{aligned}
& \left[p \alpha_1^n + \alpha_3^n (pH_n + 1) \right] e^{pH_n} \\
& + \left[-p \alpha_2^n + \alpha_4^n (1 - pH_n) \right] e^{-pH_n} \\
= & \beta_1^n \left[p \alpha_1^{n+1} + \alpha_3^{n+1} (pH_n + 1) \right] e^{pH_n} \\
& + \beta_1^n \left[-p \alpha_2^{n+1} + \alpha_4^{n+1} (1 - pH_n) \right] e^{-pH_n} \tag{A-31d}
\end{aligned}$$

where
$$\beta_1^n = \frac{E_n (1 + v_{n+1})}{E_{n+1} (1 + v_n)}$$

The above system of four equations (A-31) is solved for α^n in terms of α^{n+1} , which are presumed known. Fortunately, no algebraically cumbersome determinant computations are necessary. The symmetry in this system is such that merely adding the equations of (A-31) after appropriate sign changes, will suffice. For example, adding the four equations (A-31) as they are will leave α_3^n by itself on the left side, α_1^n , α_2^n , and α_4^n cancelling out. Changing the signs of equations (A-31a) and (A-31d) and then adding the equations (A-31), yields α_4^n by itself on the right. Some additional substituting is necessary to get α_1^n and α_2^n , namely the just acquired expressions for α_3^n and α_4^n . The results of this series of additions are the recursion formulae, which provide the basis

for the solution of the multilayer elastic problem and are the heart of the ELAST computer program (Appendix C). The recursion formulae for the α^n are:

$$4\alpha_3^n (1 - \nu_n) = 2p\alpha_2^{n+1} (1 - \beta_1^n) e^{-2pH_n} + \beta_6^n \alpha_3^{n+1} + \alpha_4^{n+1} (1 - \beta_1^n) \beta_3^n e^{-2pH_n} \quad (\text{A-32a})$$

$$4\alpha_4^n (1 - \nu_n) = 2p\alpha_1^{n+1} (\beta_1^n - 1) e^{2pH_n} + \alpha_3^{n+1} (\beta_1^n - 1) \beta_4^n e^{2pH_n} + \beta_6^n \alpha_4^n \quad (\text{A-32b})$$

$$4p\alpha_1^n (1 - \nu_n) = p\beta_2^n \alpha_1^{n+1} + p\alpha_2^{n+1} (\beta_1^n - 1) \beta_7^n e^{-2pH_n} + \beta_8^n \alpha_3^{n+1} + \beta_{10}^n \alpha_4^{n+1} e^{-2pH_n} \quad (\text{A-32c})$$

$$4p\alpha_2^n (1 - \nu_n) = p\alpha_1^{n+1} (\beta_1^n - 1) \beta_5^n e^{2pH_n} + p\beta_2^n \alpha_2^{n+1} + \beta_{11}^n \alpha_3^{n+1} e^{2pH_n} + \beta_9^n \alpha_4^{n+1} \quad (\text{A-32d})$$

$$\text{where } \beta_2^n = \beta_1^n - 4\nu_n + 3$$

$$\beta_3^n = 2pH_n - 4\nu_{n+1} + 1$$

$$\beta_4^n = 2pH_n + 4\nu_{n+1} - 1$$

$$\beta_5^n = 4\nu_n - 2pH_n - 1$$

$$\beta_6^n = \beta_1^n (3 - 4\nu_{n+1}) + 1$$

$$\beta_7^n = 4v_n + 2pH_n - 1$$

$$\begin{aligned} \beta_8^n &= (\beta_1^n - 1)(8v_n v_{n+1} - 2pH_n + 1) + 4pH_n (\beta_1^n v_{n+1} - v_n) \\ &\quad - 6 (\beta_1^n v_n - v_{n+1}) \end{aligned}$$

$$\begin{aligned} \beta_9^n &= (1 - \beta_1^n)(8v_n v_{n+1} + 2pH_n + 1) + 4pH_n (\beta_1^n v_{n+1} - v_n) \\ &\quad + 6 (\beta_1^n v_n - v_{n+1}) \end{aligned}$$

$$\begin{aligned} \beta_{10}^n &= (\beta_1^n - 1) \left[(2pH_n - 4v_{n+1})(2v_n + pH_n) + 1 \right] + 2\beta_1^n v_n \\ &\quad - 2v_{n+1} \end{aligned}$$

$$\begin{aligned} \beta_{11}^n &= (\beta_1^n - 1) \left[(4v_n - 2pH_n)(pH_n + 2v_{n+1}) - 1 \right] - 2\beta_1^n v_n \\ &\quad + 2v_{n+1} \end{aligned}$$

For convenience, the following substitutions are made in equations (A-32) to obtain the final form of the recursive equations

$$pa = x \tag{A-33a}$$

$$p^4 \alpha_1^n = -PaA_1^n J_1(x) \tag{A-33b}$$

$$p^4 \alpha_2^n = -PaA_2^n J_1(x) \tag{A-33c}$$

$$p^3 \alpha_3^n = -PaA_3^n J_1(x) \tag{A-33d}$$

$$p^3 \alpha_4^n = -PaA_4^n J_1(x) \tag{A-33e}$$

$$A_1^n = A_5^n e^{-2pH_n}$$

$$A_3^n = A_6^n e^{-2pH_n}$$

(A-34)

The A^1 constants will be in the final stress and displacement formulae. The last two substitutions [equations (A-34)] are made to remove positive exponents of "e" which during computations may become too large for the computer to properly handle. The final recursive formulae are:

$$4A_5^n (1 - \nu_n) = \beta_2^n A_5^{n+1} e^{-2ph_{n+1}} + \beta_7^n (\beta_1^n - 1) A_2^{n+1} + \beta_8^n A_6^{n+1} e^{-2ph_{n+1}} + \beta_{10}^n A_4^{n+1}$$

$$4A_2^n (1 - \nu_n) = \beta_5^n (\beta_1^n - 1) A_5^{n+1} e^{-2ph_{n+1}} + \beta_2^n A_2^{n+1} + \beta_{11}^n A_6^{n+1} e^{-2ph_{n+1}} + \beta_9^n A_4^{n+1} \quad (A-35)$$

$$4A_6^n (1 - \nu_n) = 2(1 - \beta_1^n) A_2^{n+1} + \beta_6^n A_6^{n+1} e^{-2ph_{n+1}} + \beta_3^n (1 - \beta_1^n) A_4^{n+1}$$

$$4A_4^n (1 - \nu_n) = 2(\beta_1^n - 1) A_5^{n+1} e^{-2ph_{n+1}} + \beta_4^n (\beta_1^n - 1) A_6^{n+1} e^{-2ph_{n+1}} + \beta_6^n A_4^{n+1}$$

From equation (A-27) where $n = N$ it is seen that for $\bar{\phi}$ to be bounded requires that $\alpha_1^N = 0$ and $\alpha_3^N = 0$. This implies from equations (A-33 and A-34) that

$$A_1^N = A_3^N = A_5^N = A_6^N = 0$$

Therefore, the recursive formulae [equations (A-35)] evaluated at the N-1, N interface are:

$$\begin{aligned}
 4A_5^{N-1}(1 - v_{N-1}) &= \beta_7^{N-1}(\beta_1^{N-1} - 1)A_2^N + \beta_{10}^{N-1}A_4^N \\
 4A_2^{N-1}(1 - v_{N-1}) &= \beta_2^{N-1}A_2^N + \beta_9^{N-1}A_4^N \\
 4A_6^{N-1}(1 - v_{N-1}) &= 2A_2^N(1 - \beta_1^{N-1}) + \beta_3^{N-1}(1 - \beta_1^{N-1})A_4^N \\
 4A_4^{N-1}(1 - v_{N-1}) &= \beta_6^{N-1}A_4^N
 \end{aligned} \tag{A-36}$$

Starting at the bottom interface with equations (A-36) and proceeding upward through repeated applications of equations (A-35), four expressions [equations (A-37), not shown because of their extreme length] for the top layer constants [A_2^1 , A_4^1 , A_5^1 , and A_6^1] are developed. These four new equations (obtained from compatibility) are expressed in terms of A_2^N and A_4^N . Through combining equations (A-34) [which relate A_1^1 to A_5^1 , and A_3^1 to A_6^1] and equations (A-37), the four independent (with respect to Z), arbitrary, top layer constants [A_1^1 , A_2^1 , A_3^1 , and A_4^1] are defined in terms of A_2^N and A_4^N .

To complete the solution (and in essence solve for A_2^N and A_4^N), the boundary conditions at the top layer are applied, equations (A-12 and A-13). Transforming equation (A-12) yields:

$$\begin{aligned}
 \bar{\sigma}_{zz}(p,0) &= - \int_0^a prJ_0(pr)dr = - \frac{P}{p} \int_0^a prJ_0(pr)dpr \\
 &= - \frac{P}{p} \left[prJ_1(pr) \right] \Bigg|_{r=0}^a = - \frac{Pa}{p} J_1(pa)
 \end{aligned} \tag{A-38}$$

and from equation (A-13):

$$\bar{\sigma}_{rz}(p,0) = 0 \tag{A-39}$$

Using equation (A-19), in conjunction with equations (A-28 and A-30), at $z = 0$, the following is obtained for equation (A-38).

$$p^4(\alpha_2^1 - \alpha_1^1) + p^3(1 - 2\nu_1)(\alpha_3^1 + \alpha_4^1) = -PaJ_1(pa)$$

Making the substitutions from equations (A-33), the final form of this boundary condition is:

$$A_1^1 - A_2^1 + (2\nu_1 - 1)(A_3^1 + A_4^1) = -1 \quad (A-40a)$$

Similarly for equation (A-39) the following boundary condition is derived, with the aid of equations (A-20, A-27, A-29, and A-33).

$$A_1^1 + A_2^1 + 2\nu_1(A_3^1 - A_4^1) = 0 \quad (A-40b)$$

From the previous discussion, it was shown that $[A_1^1, A_2^1, A_3^1, \text{ and } A_4^1]$ are obtained from the two non-zero bottom layer constants, A_2^N and A_4^N . Therefore equations (A-40) can be written in terms of A_2^N and A_4^N , getting

$$K_1 A_2^N + K_2 A_4^N = 0 \quad (A-41a)$$

$$K_3 A_2^N + K_4 A_4^N = -1 \quad (A-41b)$$

The introduction of the K constants provides a simplified means of solving equations (A-40) for the two bottom layer constants. By setting $A_2^N = 1$ and $A_4^N = 0$ and plugging equations (A-37, not shown) into equations (A-41), the coefficients K_1, K_3 , are obtained as the left members of equations (A-41). Similarly K_2 and K_4 are derived by setting $A_2^N = 0$ and $A_4^N = 1$. Then A_2^N, A_4^N , are obtained by solving equations (A-41). Finally, by plugging A_2^N, A_4^N into equations (A-37), we get $[A_1^1, A_2^1, A_3^1, A_4^1]$ at the top.

Next, the stress $[\sigma_{rr}(0, h_1)]$ is derived. First, some auxiliary Bessel function relationships are established.

$$\frac{d}{dx} \left[x^i J_i(x) \right] = x^i J_{i-1}(x) \quad (\text{A-42})$$

$$\frac{d}{dx} \left[x^{-i} J_i(x) \right] = -x^{-i} J_{i+1}(x) \quad (\text{A-43})$$

for $i = 0$, equation (A-43) gives

$$J_0'(x) = -J_1(x) \quad (\text{A-44})$$

and for $i = 1$, equation (A-42) becomes

$$J_1(x) + xJ_1'(x) = xJ_0(x)$$

Recalling from equation (A-33a) that $x = pr$, the above becomes

$$prJ_1'(pr) = prJ_0(pr) - J_1(pr) \quad (\text{A-45})$$

Second, some functions of ϕ are derived using the inverse transform, [i.e., L^{-1}].

$$L_0^{-1}(\bar{\phi}) = \phi = \int_0^\infty p \bar{\phi} J_0(pr) dp \quad (\text{A-46})$$

$$\text{and } \frac{\partial \phi}{\partial r} = \int_0^\infty p^2 \bar{\phi} J_0'(pr) dp = - \int_0^\infty p^2 \bar{\phi} J_1(pr) dp$$

which results in

$$\frac{1}{r} \frac{\partial \phi}{\partial r} = - \int_0^\infty p^2 \bar{\phi} \frac{J_1(pr)}{r} dp \quad (\text{A-47})$$

$$\text{and } \frac{\partial^2 \phi}{\partial r^2} = - \int_0^\infty p^3 \phi J_1'(pr) dp = - \int_0^\infty p^2 \phi pr \frac{J_1'(pr)}{r} dp$$

which when combined with equation (A-45) becomes

$$\frac{\partial^2 \phi}{\partial r^2} = \int_0^\infty p^2 \phi \frac{J_1(pr)}{r} dp - \int_0^\infty p^3 \phi J_0(pr) dp \quad (\text{A-48})$$

To find $\frac{\partial^2 \phi}{\partial z^2}$, use equations (A-46 and A-18) to obtain

$$\phi = \int_0^\infty \left[(p\alpha_1 + p\alpha_3 z)e^{pz} + (p\alpha_2 + p\alpha_4 z)e^{-pz} \right] J_0(pr) dp$$

$$\text{then } \frac{\partial \phi}{\partial z} = \int_0^\infty \left[p^2 \alpha_1 + p\alpha_3 + p^2 \alpha_3 z \right] e^{pz} + (p\alpha_4 - p^2 \alpha_2 - p^2 \alpha_4 z) e^{-pz} \left] J_0(pr) dp$$

and finally

$$\begin{aligned} \frac{\partial^2 \phi}{\partial z^2} = \int_0^\infty & \left[(2p^2 \alpha_3 + p^3 \alpha_1 + p^3 \alpha_3 z) e^{pz} \right. \\ & \left. + (p^3 \alpha_2 - 2p^2 \alpha_4 + p^3 \alpha_4 z) e^{-pz} \right] J_0(pr) dp \quad (\text{A-49}) \end{aligned}$$

To start the computation for σ_{rr} [equation (A-2)], the following expression is evaluated by substitutions from equations (A-14, A-18, A-47, A-48, and A-49).

$$\begin{aligned} \nu \nabla^2 \phi - \frac{\partial^2 \phi}{\partial r^2} = & -\nu \int_0^\infty p^3 \phi J_0(pr) dp \\ & + \nu \int_0^\infty \left[2p^2 \alpha_3 + p^3 \alpha_1 + p^3 \alpha_3 z \right] e^{pz} \\ & + (p^3 \alpha_2 - 2p^2 \alpha_4 + p^3 \alpha_4 z) e^{-pz} \left] J_0(pr) dp \end{aligned}$$

$$\begin{aligned}
& - \int_0^{\infty} \left[(p^2 \alpha_1 + p^2 \alpha_3 z) e^{pz} + (p^2 \alpha_2 + p^2 \alpha_4 z) e^{-pz} \right] \frac{J_1(pr)}{r} dp \\
& + \int_0^{\infty} p^3 \bar{\phi} J_0(pr) dp
\end{aligned}$$

By consolidating the first two terms and plugging for $\bar{\phi}$,

$$\begin{aligned}
vV^2\phi - \frac{\partial^2\phi}{\partial r^2} &= 2v \int_0^{\infty} (p^2 \alpha_3 e^{pz} - p^2 \alpha_4 e^{-pz}) J_0(pr) dp \\
& - \int_0^{\infty} \left[(p^2 \alpha_1 + p^2 \alpha_3 z) e^{pz} + (p^2 \alpha_2 + p^2 \alpha_4 z) e^{-pz} \right] \frac{J_1(pr)}{r} dp \\
& + \int_0^{\infty} \left[(p^3 \alpha_1 + p^3 \alpha_3 z) e^{pz} + (p^3 \alpha_2 + p^3 \alpha_4 z) e^{-pz} \right] J_0(pr) dp
\end{aligned}$$

Finally, using equation (A-2),

$$\begin{aligned}
\sigma_{rr}(r, z) &= \frac{\partial}{\partial z} \left(vV^2\phi - \frac{\partial^2\phi}{\partial r^2} \right) \\
&= 2v \int_0^{\infty} (p^3 \alpha_3 e^{pz} + p^3 \alpha_4 e^{-pz}) J_0(pr) dp \\
&+ \int_0^{\infty} \left[(p^4 \alpha_1 + p^4 \alpha_3 z + p^3 \alpha_3) e^{pz} \right. \\
&+ \left. (p^3 \alpha_4 - p^4 \alpha_2 - p^4 \alpha_4 z) e^{-pz} \right] J_0(pr) dp \\
&- \int_0^{\infty} \left[(p^3 \alpha_1 + p^3 \alpha_3 z + p^2 \alpha_3) e^{pz} \right. \\
&+ \left. (p^2 \alpha_4 - p^3 \alpha_2 - p^3 \alpha_4 z) e^{-pz} \right] \frac{J_1(pr)}{r} dp
\end{aligned}$$

Combining terms,

$$\begin{aligned} \sigma_{rr} = & \int_0^{\infty} \left\{ \left[p^4 \alpha_1 + p^3 \alpha_3 (1 + 2\nu + pz) \right] e^{pz} \right. \\ & + \left. \left[- p^4 \alpha_2 + p^3 \alpha_4 (1 + 2\nu - pz) \right] e^{-pz} \right\} J_0(pr) dp \\ & - \int_0^{\infty} \left\{ \left[p^3 \alpha_1 + p^2 \alpha_3 (1 + pz) \right] e^{pz} \right. \\ & + \left. \left[- p^3 \alpha_2 + p^2 \alpha_4 (1 - pz) \right] e^{-pz} \right\} \frac{J_1(pr)}{r} dp \end{aligned}$$

Evaluating σ_{rr} at the point of interest (i.e., $r = 0$, $z = h_1$) and noting that at $r = 0$, $J_0(0) = 1$

$$\text{and also } \lim_{r \rightarrow 0} \frac{J_1(pr)}{r} = \frac{p}{2}$$

The following expression for σ_{rr} is obtained

$$\begin{aligned} \sigma_{rr}(0, h_1) = & \int_0^{\infty} \left\{ \left[p^4 \alpha_1^1 + p^3 \alpha_3^1 (1 + 2\nu_1 + ph_1) \right] e^{ph_1} \right. \\ & + \left. \left[- p^4 \alpha_2^1 + p^3 \alpha_4^1 (1 + 2\nu_1 - ph_1) \right] e^{-ph_1} \right\} dp \\ & - \frac{1}{2} \int_0^{\infty} \left\{ \left[p^4 \alpha_1^1 + p^3 \alpha_3^1 (1 + ph_1) \right] e^{ph_1} \right. \\ & + \left. \left[- p^4 \alpha_2^1 + p^3 \alpha_4^1 (1 - ph_1) \right] e^{-ph_1} \right\} dp \end{aligned}$$

where the superscript 1 denotes the 1st layer

$$= 1/2 \int_0^{\infty} \left\{ \left[p^4 \alpha_1^1 + p^3 \alpha_3^1 (1 + 4\nu_1 + ph_1) \right] e^{ph_1} \right. \\ \left. + \left[- p^4 \alpha_2^1 + p^3 \alpha_4^1 (1 + 4\nu_1 - ph_1) \right] e^{-ph_1} \right\} dp$$

Substitution from equation (A-33) yields

$$\sigma_{rr}(0, h_1) = -\frac{Pa}{2} \int_0^{\infty} \left\{ \left[A_1^1 + A_3^1 (1 + 4\nu_1 + ph_1) \right] e^{ph_1} \right. \\ \left. + \left[- A_2^1 + A_4^1 (1 + 4\nu_1 - ph_1) \right] e^{-ph_1} \right\} J_1(x) dp$$

Substitution from equation (A-34) yields

$$\sigma_{rr}(0, h_1) = -\frac{P}{2} \int_0^{\infty} \left[A_5^1 - A_2^1 + (A_6^1 + A_4^1)(4\nu_1 + 1) \right. \\ \left. + ph_1 (A_6^1 - A_4^1) \right] e^{-ph_1} J_1(x) dx \quad (A-50)$$

Equation (A-50) is used in the ELAST program to evaluate $\sigma_{rr}(0, h_1)$ - referred to as σ in other parts of this report. The integration is done numerically, using Gaussian quadratures, as will be explained later.

Now, the expression for the downward displacement at the top of the layered system is derived. Starting with equation (A-21) and substituting from equation (A-27 and A-29) at $z = 0$, the following results.

$$\bar{w}(p, 0) = \frac{1 + \nu_1}{E_1} \left[(1 - 2\nu_1) (p^2 \alpha_1^1 + 2p \alpha_3^1 + p^2 \alpha_2^1 - 2p \alpha_4^1) \right]$$

$$\begin{aligned}
& + (2\nu_1 - 2)(p^2\alpha_1^1 + p^2\alpha_2^1) \\
= & \frac{1 + \nu_1}{E_1} \left[-p^2\alpha_1^1 - p^2\alpha_2^1 + 2p(\alpha_3^1 - \alpha_4^1)(1 - 2\nu_1) \right] \\
= & \frac{1 + \nu_1}{p^2 E_1} \left[-p^4\alpha_1^1 - p^4\alpha_2^1 + 2p^3(\alpha_3^1 - \alpha_4^1)(1 - 2\nu_1) \right]
\end{aligned}$$

Substitutions from (A-33) gives

$$\bar{w}(p,0) = \frac{Pa(1 + \nu_1)}{p^2 E_1} \left[A_1^1 + A_2^1 + 2(2\nu_1 - 1)(A_3^1 - A_4^1) \right] J_1(x)$$

Performing the inverse transform yields

$$w(r,0) = \int_0^\infty p \bar{w}(p,0) J_0(pr) dp$$

$$\text{and } w(0,0) = \int_0^\infty p \bar{w}(p,0) dp$$

Thus,

$$w(0,0) = \frac{Pa(1 + \nu_1)}{E_1} \int_0^\infty \left[A_1^1 + A_2^1 + (4\nu_1 - 2)(A_3^1 - A_4^1) \right] \frac{J_1(x)}{p} dp$$

and finally the formulae used in the computer program:

$$w(0,0) = \frac{Pa(1 + \nu_1)}{E_1} \int_0^\infty \left[A_1^1 + A_2^1 + (4\nu_1 - 2)(A_3^1 - A_4^1) \right] \frac{J_1(x)}{x} dx$$

(A-51)

Elsewhere in this report $w(0,0)$ is referred to as δ .

The integration of equations (A-50) and (A-51) is performed numerically by means of Gaussian quadratures using roots of Legendre polynomials [References 8, 9, and 10]. Although Gaussian integration is done between finite limits, it can be used for improper integrals such as equations (A-50) and (A-51), whose integrands approach zero for sufficiently large values of the variable of integration x . In the program ELAST, the table of Reference 10 for $n = 16$ is used; and integration is over either three or four intervals of x , as determined by a test on the negative exponential factor of equation (A-50).

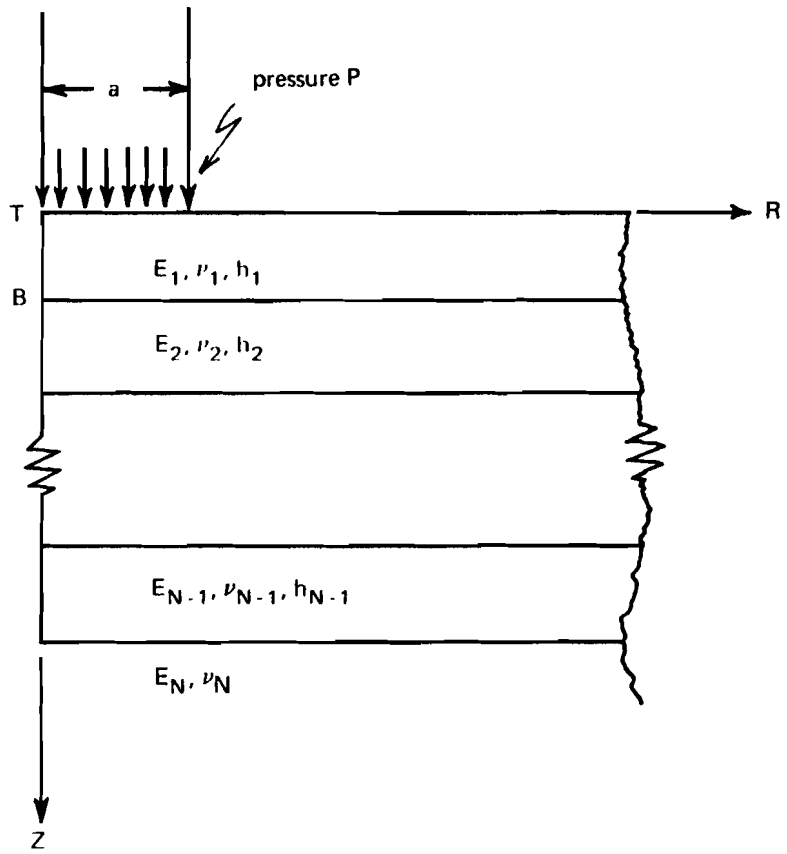


Figure A-1. Multilayer elastic half space.

Appendix B

“EXACT” SOLUTIONS FOR THE WESTERGAARD IDEALIZATION

Computation of the Westergaard functionals, k_w^2 and k_s^1 , requires solution of the Westergaard problem and solution of an elastic layer problem, such that, a k is computed which produces identical results for equations (1 and 3) and (2 and 4). Equations (3 and 4) are the “exact” solution for the layer elastic problem, but equations (1 and 2) are only first order approximations for the solution of a plate on a fluid foundation [Reference 11]. Equation (1 and 2) appears to be valid for the traditional applications of a rigid layer over a relatively soft subgrade. For pavements where this distinction does not exist or is marginal, erroneous results are obtained. While this problem may be of little practical significance because most applications provide a clear distinction between subgrade and pavement surface, it was deemed necessary that more refined theories be used for derivation of the functionals. Two refined approaches were taken resulting in two versions of the ELAST computer program. The first involves adding additional terms to equations (1 and 2); these additional terms were included in Westergaard’s original work [Reference 11] but are generally ignored in normal applications. The second approach is completely different from the first, being based on the solution for an elastic layer media presented in Appendix A.

1. EXTENDED WESTERGAARD APPROACH

The extension of Westergaard’s simplified equations (1 and 2) – for solving the problem of a laterally infinite elastic plate resting on a fluid (Figure 1) – will not be shown here, since some background is required and it is already in the literature [References 12, 13, and 14]. Reference 12 furnishes the background in plate theory, and Reference 13 addresses itself to the particular problem while Reference 14 may provide additional support.

The two equations used for maximum lateral stress and peak displacement are, respectively, equations (5.2) and (4.6) of Reference 13. These along with some auxiliary equations follow.

Equation (5.2) is

$$\sigma_{rr} = \frac{3F(1 + \nu)Kei' b}{\pi b h^2}$$

where $F = \pi P a^2$, the total force applied to the plate

$$b = a' \left(\frac{k}{D}\right)^{1/4}$$

$$D = \frac{Eh^3}{12(1 - \nu^2)}, \text{ known as the flexural rigidity}$$

$$a' = \begin{cases} \sqrt{1.6a^2 + h^2} & \text{-.675h, if } a < 1.724h \\ a & \text{, otherwise} \end{cases}$$

$k =$ density of supporting fluid (the Westergaard constant)

or alternatively

$$\sigma_{rr} = \frac{3Pa^2(1 + \nu)Kei' b}{bh^2} \quad (B-1)$$

Equation (4.6) is

$$w = \frac{Pa^2(1 + \nu)Ker' b}{ka'^2} \quad (B-2)$$

The Ker and Kei functions whose derivatives appear in equations (B-1) and (B-2) are:

$$\begin{aligned} \text{Ker } b = & -g + \frac{\pi b^2}{16} + \frac{2g - 3}{128} b^4 - \frac{\pi b^6}{9216} + \frac{25 - 12g}{1769472} b^8 \\ & + \frac{\pi b^{10}}{58982400} + \frac{20g - 49}{42467328000} b^{12} \end{aligned}$$

$$\begin{aligned} \text{Ker}' b = & -\frac{1}{b} + \frac{\pi b}{8} + \frac{4g - 5}{64} b^3 - \frac{\pi b^5}{1536} + \frac{47 - 24g}{442368} b^7 \\ & + \frac{\pi b^9}{5898240} \end{aligned}$$

$$\begin{aligned} \text{Kei } b = & -\frac{\pi}{4} + \frac{1 - g}{4} b^2 + \frac{\pi b^4}{256} + \frac{6g - 11}{13824} b^6 \\ & - \frac{\pi b^8}{589824} + \frac{1.37 - .6g}{8847360} b^{10} + \frac{\pi b^{12}}{8493465600} \end{aligned}$$

$$\begin{aligned} \text{Kei}' b = & \frac{b(1 - 2g)}{4} + \frac{\pi b^3}{64} + \frac{3g - 5}{1152} b^5 - \frac{\pi b^7}{73728} \\ & + \frac{13.1 - 6g}{8847360} b^9 \end{aligned}$$

where $g = \gamma + \ln \frac{b}{2} = .57722 + \ln \frac{b}{2}$

so that $\frac{\partial g}{\partial b} = \frac{1}{b}$

The formulae given here for the derivatives Ker' b and Kei' b contain the number of terms currently used in the "red deck" computer program (described in Section B-3).

2. ELASTICITY APPROACH

Solving the Westergaard idealization (Figure 1) using an elasticity approach, employs the same set of differential equations and the same Hankel transform method used in Appendix A for solving the multilayer problem. Only the boundary conditions on the bottom of the elastic layer are different. This approach is felt to be more accurate than the extended Westergaard approach.

As before, a circular pressure load of radius a rests atop the elastic layer of thickness h . Again, the differential equations (A-1 to A-6) apply, along with equation (A-7) and boundary conditions (A-12 and A-13). In addition, we have the following boundary conditions at the plate's bottom surface.

$$\sigma_{zz}(r,h) = -kw(r,h) \quad (B-3)$$

$$\sigma_{rz}(r,h) = 0 \quad (B-4)$$

where k is the fluid density.

Applying the Hankel transform $[L_0]$,

$$\bar{\sigma}_{zz}(p,z) = \int_0^\infty p\sigma_{zz}(r,z)J_0(pr)dr$$

Using equation (A-19) and substitutions from equations (A-28 and A-30), the following is derived.

$$\begin{aligned} \bar{\sigma}_{zz}(p,z) = p^2 & \left[-\alpha_1 p + \alpha_3(1 - 2\nu - pz) \right] e^{pz} \\ & + p^2 \left[\alpha_2 p + \alpha_4(1 - 2\nu + pz) \right] e^{-pz} \quad (B-5) \end{aligned}$$

Similarly, using equations (A-21, A-27, and A-29) yields

$$\bar{w}(p, z) = \frac{1 + \nu}{E} \left\{ \left[-p^2 \alpha_1 + p \alpha_3 (2 - 4\nu - pz) \right] e^{pz} + \left[-p^2 \alpha_2 + p \alpha_4 (4\nu - 2 - pz) \right] e^{-pz} \right\} \quad (B-6)$$

Applying equation (B-3) in transform space with substitution from equations (B-5 and B-6) gives

$$\begin{aligned} & \left[-\alpha_1 p^2 + \alpha_3 p (1 - 2\nu - ph) \right] e^{ph} \\ & + \left[\alpha_2 p^2 + \alpha_4 p (1 - 2\nu + ph) \right] e^{-ph} \\ = & - \frac{k(1 + \nu)}{E} \left\{ \left[-p \alpha_1 + \alpha_3 (2 - 4\nu - ph) \right] e^{ph} + \left[-p \alpha_2 + \alpha_4 (4\nu - 2 - ph) \right] e^{-ph} \right\} \quad (B-7) \end{aligned}$$

Using substitutions [equations (A-33)] and

$$L = \frac{k(1 + \nu)}{E},$$

equation (B-7) becomes

$$\begin{aligned} & \left\{ -A_1 (p + L) + A_3 \left[(1 - 2\nu - ph)(p + L) + L(1 - 2\nu) \right] \right\} e^{ph} \\ & + \left\{ A_2 (p - L) + A_4 \left[(1 - 2\nu + ph)(p - L) - L(1 - 2\nu) \right] \right\} e^{-ph} = 0 \quad (B-8) \end{aligned}$$

Next, the boundary condition [equation (B-4)] is applied using equations (A-20, A-27, and A-29).

$$\left[p\alpha_1 + \alpha_3(2\nu + ph) \right] e^{ph} + \left[p\alpha_2 + \alpha_4(ph - 2\nu) \right] e^{-ph} = 0 \quad (\text{B-9})$$

Using equations (A-33) and multiplying by p^3 , equation (B-9) gives

$$\left[A_1 + A_3(2\nu + ph) \right] e^{ph} + \left[A_2 + A_4(ph - 2\nu) \right] e^{-ph} = 0 \quad (\text{B-10})$$

The two boundary conditions on top of the plate are the same as those of Appendix A [equations (A-40)] and are as follows.

$$A_1 - A_2 + (2\nu - 1)(A_3 + A_4) = -1 \quad (\text{B-11})$$

$$A_1 + A_2 + 2\nu(A_3 - A_4) = 0 \quad (\text{B-12})$$

This system of equations [equations (B-8, B-10, B-11, and B-12)] is now solved for the unknown constants (A). From equations (B-11 and B-12)

$$2A_1 = (1 - 4\nu)A_3 + A_4 - 1 \quad (\text{B-13})$$

$$2A_2 = (4\nu - 1)A_4 - A_3 + 1 \quad (\text{B-14})$$

Substituting equations (B-13 and B-14) into equation (B-10):

$$A_3 = \frac{(1 - \Lambda_4)(1 - e^{-2ph}) - 2ph\Lambda_4 e^{-2ph}}{1 - e^{-2ph} + 2ph} \quad (\text{B-15})$$

Substitution of equations (B-13, B-14, and B-15) into equation (B-8) yields after a rather lengthy algebraic process

$$A_4 = \left\{ (1 - e^{-2ph}) \left[p + 2L(1 - \nu) \right] + 2p^2 h e^{-2ph} \right\} \div \left\{ p + 2L(1 - \nu) + 2p e^{-2ph} \left[4hL(1 - \nu) - 2p^2 h^2 - 1 \right] + \left[p - 2L(1 - \nu) \right] e^{-4ph} \right\}$$

A_1 , A_2 , and A_3 are then computed using equations (B-13, B-14, and B-15). A_5 and A_6 are defined as before using equations (A-34).

Having now obtained the layer constants [$A_1 \dots A_6$] the expressions for $\sigma_{rr}(0, h)$ [equation (A-50)] and $w(0,0)$ [equation (A-51)] can be evaluated. This is accomplished in a manner similar to that described in Appendix A.

3. COMPARISON OF APPROACH 1 AND 2

The variation of results, for the two approaches is demonstrated using the pavement sections of Table B-1. These sections are designed to mathematically test the prediction techniques, which results in rather strange pavement systems. Two separate computer program were written to solve for the stress functionals k_s^1 and k_s^2 - the "red deck" employs the extended Westergaard approach while the "brown deck" employs the elasticity approach. The first and second columns of Table B-2 show the stress functional, k_s^1 , computed by the "red and brown decks". For pavement systems which are normally encountered, there is satisfactory agreement between the two approaches. For systems which probably have no significance, major discrepancies appear. While current applications produce no need for the "brown deck" refinements, it is felt that usage of the "brown deck" with its inherently more rigorous approach avoids any potential future problems and that the additional

computer costs^k incurred are of no significance with respect to the anticipated number of runs. All computations presented elsewhere in this report are accomplished using the "brown deck." Column three of Table B-2 shows the stress functional k_s^2 . The difference between k_s^2 and k_s^1 is a measure of the error incurred when equation (2) is used to predict the stress σ for a Westergaard idealization, instead of either the "red or brown deck."

^k Cost of running the "brown deck" is approximately 3 times that of the "red."

Table B-1. Mathematically Selected Pavement Sections

Section Number	Number of Layers in the Pavement Section ^d									
	1	2	3	4	5	6	7	8	9	10
1	3 x 10 ⁶ ^b 0.15 ^c 12 ^d	10 x 10 ³ 0.2 24	5 x 10 ³ 0.25 36	500 0.4						
2	3 x 10 ⁶ 0.15 12	5 x 10 ⁴ 0.2 24	2.5 x 10 ³ 0.25 36	500 0.40						
3	8 x 10 ⁴ 0.4 16	4 x 10 ⁴ 0.2 32	2 x 10 ⁴ 0.3 48	2 x 10 ³ 0.4						
4	5 x 10 ⁶ 0.15 6	1.5 x 10 ³ 0.3 16	3 x 10 ⁶ 0.4 6	3 x 10 ³ 0.1						
5	7 x 10 ³ 0.4 12	5 x 10 ³ 0.2								
6	4 x 10 ⁶ 0.2 3	3 x 10 ³ 0.4 16	3 x 10 ⁶ 0.1 5	1 x 10 ³ 0.3 18	3 x 10 ⁶ 0.1 4	500 0.4				
7	3 x 10 ⁶ 0.2 6	4 x 10 ⁴ 0.4 20	3 x 10 ⁴ 0.3 16	2 x 10 ⁴ 0.1 10	1.5 x 10 ⁴ 0.3 20	10 x 10 ⁴ 0.2 15.0	5 x 10 ³ 0.4 17.0	2 x 10 ³ 0.15 30	1 x 10 ³ 0.3 14	500 0.4
8	4 x 10 ⁴ 0.4 20	3 x 10 ⁴ 0.3 16	2 x 10 ⁴ 0.1 10	1.5 x 10 ⁴ 0.3 20	1.0 x 10 ⁴ 0.2 15	5 x 10 ³ 0.4 17	2 x 10 ³ 0.15 30	1 x 10 ³ 0.3 14	500 0.4	
9	1 x 10 ³ 0.3 40	4 x 10 ⁴ 0.1 12	500 0.2							
10	10 x 10 ³ 0.3 12	3 x 10 ⁶ 0.15 6	15 x 10 ³ 0.4 18	20 x 10 ³ 0.3						
11	30 x 10 ³ 0.2 36.0	20 x 10 ³ 0.0 15.0	15 x 10 ³ 0.0 17.0	5 x 10 ³ 0.5						
12	5 x 10 ³ 0.2 12	5 x 10 ³ 0.2								

^d Layers are numbered starting at the top of the section.
^b Young's modulus in "psi" for the layer.
^c Poisson's ratio for the layer.
^d Layer thickness in inches.

Table B-2. Comparison of Stress Functionals

Section Number	k_s^1		k_s^2 Equation (2)
	“Brown Deck”	“Red Deck”	
1	30	30	34
2	894	930	1,045
3	39,000	>99,999	>99,999
4	61	63	48
5	$>1.0 \times 10^6$	$>10^6$	9,619
6	206	195	180
7	2,314	2,628	1,824
8	$>10^6$	>99,999	>99,999
9	NP ^a	NP ^a	NP ^a
10	NP	NP	NP
11	$>10^6$	$>10^6$	>99,999
12	$>10^6$	74,197	7,031

^a Compressive stress in bottom fiber of plate: solution not permissible.

Appendix C

ELAST COMPUTER PROGRAM

The equations derived in Appendices A and B were used as a framework to build the ELAST program. This code solves for the five functionals described in Section II: k_w^1 , k_w^2 , k_w^3 , k_s^1 , and k_s^2 . In addition, ELAST computes the responses for the elastic layer and Westergaard idealizations - equations (1 to 4). The program computes these quantities for up to 10 layers of material for any specified radius and magnitude of load. The input consists primarily of specification for each layer of E, ν , and thickness. The user manual for the ELAST computer program is shown in Figure C-1. Three different card formats are required to define a single problem. As many problems as desired may be stacked one behind another.

1. Example Problem

The following input data for the ELAST program was obtained from section A2 of Figure 5 and was used to generate the results shown in Figure C-2.

Card Column	5	10	20	30
	SECTION A2 TABLE 5 CRUSHED LIMESTONE AND GRAVEL SUBGRADE			
	3	42.77	15.0	300.0
	750000.	0.2	8.0	
	33000.	0.3	24.0	
	6000.	0.3	24.0	
	STOP			

2. Discussion of Output

The output consists of a reflection of the input (i.e., The input data is written out when read to aid in debugging). Also output are the functionals and the σ and δ predicted by the elastic layer or Westergaard analyses. The output is shown in Figure C-2. The ELAST results are shown in tabular form.

The first row of the table [title: MODULUS OF SUBGRADE REACTION] has the units of pounds per cubic inch. The concept of replacing the

stiffness of the various subgrade layers with a single constant comes from Westergaard. The advantage of this is reducing the multilayered soil problem to that of a plate on an elastic foundation. The functionals calculated in the code will be different depending on the criteria employed, thus, providing several ways to relate the elastic layer and Westergaard solutions. The second row [title: STRESS IN BOTTOM FIBER OF FIRST LAYER] presents the stress calculated at the bottom extreme fiber of the first layer under the center of the load. This is the maximum tensile stress, hence, a design parameter for a rigid pavement. Row three [title: DEFLECTIONS AT SURFACE UNDER LOAD] contains the deflections at the surface under the center of the load in inches.

The manner in which rows one, two, and three are filled in is as follows. Solution of the elastic layer equations (3 and 4) is contained in the first column. This stress and deflection will be used to calculate all the functionals except k_w^1 . Row one will be blank as it has no meaning for the elastic layer solution.

If a value for the measured k is input (Format B, columns 31 to 40), the traditional Westergaard solution for maximum stress and deflection will be calculated, i.e., equations (1 and 2). These values will be in column 2 of the tabular output (labeled: WESTERGAARD SINGLE TERM).

The results obtained by employing the k_w^1 functional are shown in column 3 (labeled: SUBGRADE DISPLACEMENT FUNCTIONAL). k_w^1 is obtained by stripping off the first layer of the soil/pavement system, loading it with a uniform pressure of ($P = 1$ psi) uniformly distributed over a 30-inch diameter circle. The resulting deflection is inverted to obtain the modulus, k_w^1 . k_w^1 is used to calculate the stress, row 2, and deflection, row 3. These responses are calculated using Westergaard equations (1 and 2). Equations (1 and 2) were used for the sole purpose of producing answers that would duplicate a hand calculation. To obtain a more accurate solution replace the subroutines WSTRES with XACTST and WDELTA with XACTDF (see Figure C-3). Substituting these subroutines, containing the "exact" Westergaard equations, will make little difference for the "typical" concrete pavement.

The results obtained by employing the k_s^1 and k_w^2 functionals are shown in columns 4 and 5, respectively (labeled: WESTERGAARD EXACT EQNS). k_s^1 is defined as the modulus that will produce the same stress from the Westergaard equation as that computed at the bottom of the first layer in the elastic layer analysis. It provides a means for relating the elastic layer solution to the Westergaard solution. This functional is calculated by: (1) assuming a k_s^1 , (2) solving the "exact" Westergaard stress equation with the assumed k_s^1 , (3) comparing Westergaard stress with elastic layer stress, (4) if the same, end solution cycle; or if different, go to step (1). k_s^1 is used to calculate the stress, row 2; row 3 is inapplicable. The stress shown is identical to the elastic layer response.

Functional k_w^2 , fifth column, is defined as the modulus that will produce the same deflection from the Westergaard equation as that computed at the surface of the elastic layer analysis. It provides a third method of relating elastic layer analyses with those of Westergaard. This functional is calculated by: (1) assuming a k_w^2 , (2) solving the "exact" Westergaard deflection equation, (3) comparing the Westergaard deflection with the elastic layer deflection, (4) if the same, stop; if different, go to step (1) of the solution cycle. The deflection shown is identical to the elastic layer response.

Columns 6 and 7 contain the functionals k_s^2 and k_w^3 , respectively (labeled: WESTERGAARD 1 TERM EQNS). k_s^2 is solved by inverting equation (2). k_w^3 is solved by an iteration procedure similar to that used for k_s^1 and k_w^2 . These functions were included in the table to provide a measure of the difference between the "exact" and single term Westergaard equations.

3. Program Organization

ELAST is written in FORTRAN IV and is approximately 1,000 cards long. The code requires 11,000 decimal words to execute on a CDC 6600 and has been successfully run on the CDC 6600, UNIVAC 1110, and IBM 370 computers. Figure C-3 shows the program's organizational structure. A brief description of each subroutine follows.

1. ELAST reads input and calls subroutines.
2. ELLAY solves equations (3 and 4) for σ and δ .
3. WSTRES and WDELTA solve the single term Westergaard stress and deflection equations (1 and 2). To compute the "exact" Westergaard σ and δ , replace these routine with ones shown in dashed boxes.
4. WESCON computes the constants used in the "exact" Westergaard equations.
5. KW2, KW3, KS1, KS2, and KW1, solve for the functions as indicated by their name.
6. WSTRF sets some Westergaard constants.
7. BESSEL computes values for the Bessel functions.
8. RCUR solves the recursive equations of the elasticity solution.

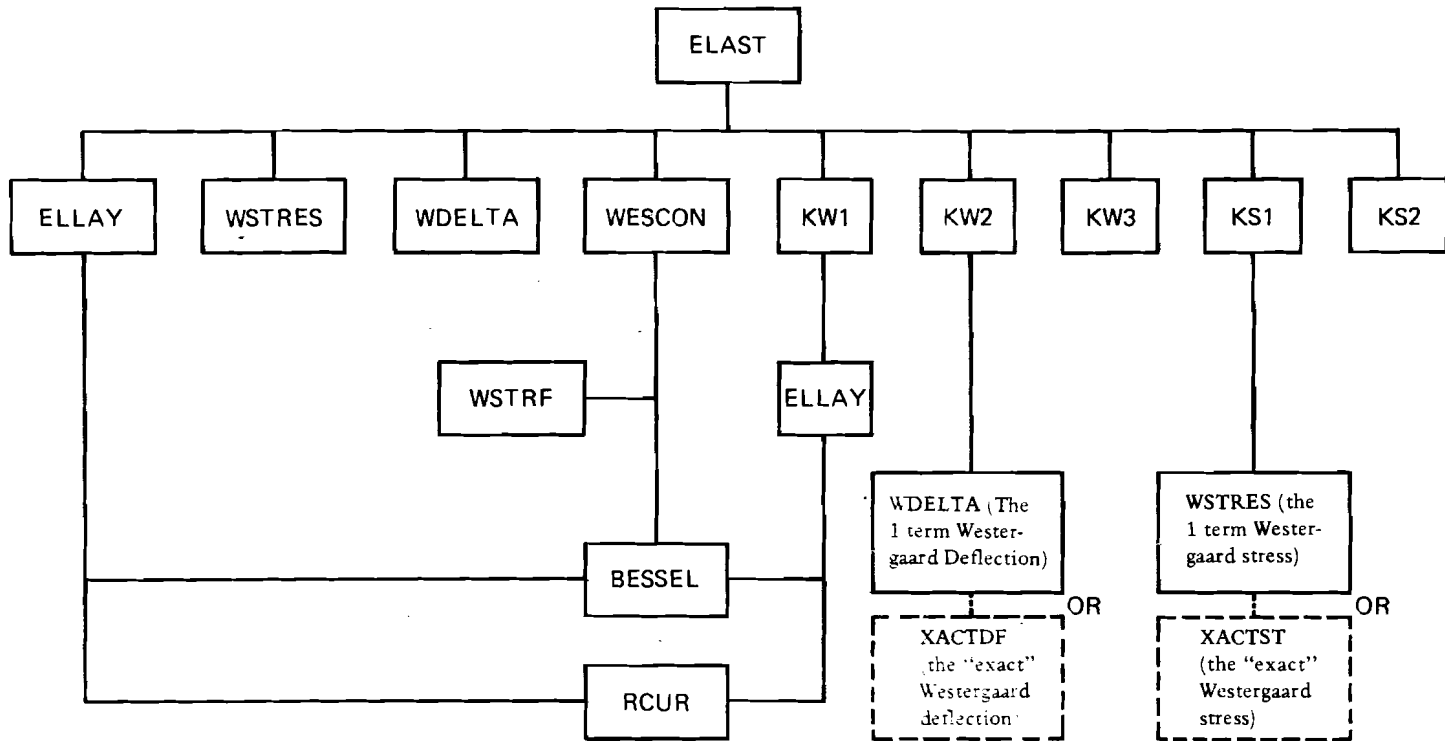


Figure C-3. Subroutine Organization for ELAST Program.

LIST OF SYMBOLS

δ	Peak deflection in first (top) pavement layer
δ_2	Peak deflection in second pavement layer
N	Number of layers occurring in an elastic layer idealization
P	Pressure
a	Load radius
E	Young's modulus
E_n	Young's modulus for the nth pavement layer
ν	Poisson's ratio
ν_n	Poisson's ratio for the nth pavement layer
h	Layer thickness
h_n	Layer thickness for the nth pavement layer
σ	Maximum tensile stress in first (top) pavement layer
k	Westergaard, subgrade stiffness parameter
A_1^n	Solution constants for the nth pavement layer (i=1,6)
p	Transform parameter derived from solution of elastic layer idealization
J_1, J_0	Bessel function
k_w^1, k_w^2, k_w^3	Westergaard displacement functionals
k_s^1, k_s^2	Westergaard stress functionals
R, Z, θ	Coordinate directions for a cylindrical coordinate system

REFERENCES

1. Westergaard, H.M., "New Formulas for Stresses in Concrete Pavements of Airfields," Transactions American Society of Civil Engineers, pp 425-444, 1947.
2. Peutz, M.G.F., et al., "BISTRO: Computer Program for Layered Systems Under Normal Surface Loads," Koninklijke/Shell Laboratorium, Amsterdam, 1968.
3. Michelow, J., "Analysis of Stresses and Displacements in an n-layered elastic system under a load uniformly distributed on a circular area," California Research Corporation, Richmond, CA, Sep 24, 1963.
4. Harrison, W., et al., "Computer Programs for Circle and Strip Loads on Layered Anisotropic Media," Division of Applied Geomechanics, Commonwealth Scientific and Industrial Research Organization, Australia 1972.
5. Crawford, J. and M.G. Katona, "State-of-the-Art for Prediction of Pavement Response," Report No. FAA-RD-75-183, Federal Aviation Administration, Washington, D.C., Sep 1975.
6. Love, A., A Treatise on the Mathematical Theory of Elasticity, Dover Publications, New York, 1944, pp 275-276.
7. Tranter, C.J., Integral Transforms in Mathematical Physics, John Wiley & Sons, New York, 1959, Sec. 4.1 and 4.2.
8. Ford, L.R., Differential Equations, McGraw-Hill, New York, 1933. Chapter IX.
9. National Bureau of Standards, Handbook of Mathematical Functions, AMS55, Table 25.4, pp 916-919. Washington DC, 1964.
10. ———. Tables of Functions and of Zeros of Functions, AMS37, Washington DC, 1954.
11. Westergaard, H.M., "Stresses in Concrete Runways of Airports," Proceedings, Highway Research Board, 19th annual meeting, 1939.
12. Timoshenko, S., and Woinowsky-Krieger, S., Theory of Plates and Shells, McGraw-Hill Book Company, New York, 1965.
13. Wyman, M. "Deflections of an Infinite Plate," Canadian Journal of Research, 1950.
14. Watson, G.N., A treatise on the Theory of Bessel Functions, Cambridge University Press, London, 1966.